

# 1 Chapter 3.6

## 2 Electrodynamic coupling between

### 3 Ganymede and the Jovian ionosphere

4 Bertrand Bonfond, Philippe Zarka

#### 5 3.6.1 Introduction

6 Having conductive interiors and/or ionospheres, the Galilean satellites are in electrodynamic inter-  
7 action with the fast-rotating Jovian magnetic field and magnetosphere, in which they are embedded.  
8 In the inner Jovian magnetosphere, within the orbit of Ganymede, the magnetic pressure of the ro-  
9 tating flow is larger than its ram pressure (except in the near equatorial current sheet at Ganymede's  
10 orbit) and the flow is sub-Alfvénic [Kivelson and Bagenal, 2014]. The flow–obstacle interactions gen-  
11 erate both local and distant effects. In this chapter, we do not focus on the local interaction, which  
12 is covered in [Chapter 3.1 \(Kivelson\)](#), but we will zoom out and explore the outcome of this inter-  
13 action further down the disturbed magnetic field lines. There, the electrodynamic satellite–Jupiter  
14 interaction takes the form of transverse perturbations of the Jovian magnetic field propagating away  
15 from the satellite along Jovian magnetic field lines at the Alfvén velocity, in both hemispheres down  
16 to the Jovian ionosphere. These perturbations are called Alfvén waves and their envelopes Alfvén  
17 wings, primarily theorized by Neubauer [1980, 1998].

18 As these waves propagate along the magnetic field lines, they initiate a long chain of processes  
19 and generate a variety of signatures associated with this of the long-range interaction, as summa-  
20 rized on Figure 3.1. Some of them, noted in white, have already been observed at Ganymede, while  
21 other are expected to take place because they have been identified at Io (in cyan). Ganymede's  
22 magnetosphere forms a large obstacle for Jupiter's magnetospheric plasma and magnetic field rotat-

ing with the planet. Its motion relative to the plasma launches large scale Alfvén waves, which then undergo some turbulent filamentation, and partial reflections at the Alfvén velocity gradients (either at the plasma sheet boundary or at the Jovian ionosphere). These waves ultimately enter a regime (mostly inertial Alfvén waves) in which they can accelerate charged particles (section 3.6.4). Part of them hit the atmosphere, exciting and ionizing neutral atoms and molecules, which generates specific auroral emissions, called the Ganymede footprint (section 3.6.2), as they de-excite. Another part of the accelerated electrons bounces due to the magnetic mirror effect. The resulting upgoing electron distribution is far from Maxwellian as it lacks the electrons with small pitch angle which have precipitated into the atmosphere, causing the feature called a loss-cone in the velocity space ( $v_{\parallel}, v_{\perp}$ ). This feature notably displays a positive gradient of the electron distribution function (or phase space density  $f(v_{\parallel}, v_{\perp})$ ) toward increasing perpendicular velocities  $v_{\perp}$ . This positive gradient is the free energy source of the Cyclotron-Maser instability (CMI) mechanism [Zarka, 1998; Hess, Mottez and Zarka, 2007; Hess et al., 2008], through which the perpendicular energy of electrons in cyclotron motion around the magnetic field lines is directly and collectively transferred to electromagnetic radio waves having this same cyclotron frequency ( $f_{ce} = eB/2\pi m_e$ ). The corresponding electrons are said « resonant » and the wave is hugely amplified, either causing the electron distribution to relax toward a Maxwellian one, or trapping resonant electrons in the wave electric field, and in both cases quenching the instability [Le Quéau, 1988]. Radio emissions are further detailed on section 3.6.3.

Because Io is closer to Jupiter, where the magnetic field magnitude is larger than at Ganymede ( $\sim 2000$  nT at Io compared to  $\sim 100$  nT at Ganymede), and embedded into the dense plasma torus stemming from the moon’s outstanding volcanism, all the outcome of the moon-magnetosphere interaction are magnified there. Hence many of the phenomena related to the moon-magnetosphere interactions were first unveiled at Io before they were found to be also applicable at Ganymede. These distant consequences are key to study these interactions because they often are the only way to get information in absence of a spacecraft measuring directly the local environment.

For example, it was the intense radio emissions related to Io that first revealed that this moon was playing such an important role in the Jovian magnetosphere. Over half a century ago, Bigg [1964] noticed that the recently discovered and variable, Jovian decametre (DAM) radio emission showed maximum occurrence at specific orbital phases of Io ( $\Phi_{Io}$ ) around Jupiter as seen from a terrestrial observer ( $\sim 90^\circ$  and  $\sim 240^\circ$  from the anti-observer’s position – Figures 3.3a and 3.2b,c).

The picture grew in complexity as spacecraft brought new pieces of information on the Jovian

55 system, starting from the simpler unipolar inductor model [Goldreich and Lynden-Bell, 1969], to  
 56 the Alfvén wing theory [Neubauer, 1980] and then all its subsequent developments, involving the  
 57 propagation and reflections of the Alfvén waves [Gurnett and Goertz, 1981; Jacobsen et al., 2007,  
 58 2010; Hinton et al., 2019], their turbulent filamentation [Chust et al., 2005] or their capability to  
 59 accelerate particles [Jones and Su, 2008; Hess et al., 2010; Hess, Bonfond, Chantry, Gérard, Grodent,  
 60 Jacobsen and Radioti, 2013; Damiano et al., 2019].

61 The arrival of Juno around Jupiter and the traversal of the field lines connected to the Io footprint  
 62 at high latitude offered a brand new perspective on the richness of the wave-particle interactions  
 63 resulting from the moon-magnetosphere couplings. The importance of Alfvén waves undergoing a  
 64 turbulent cascade and accelerating electrons along the magnetic field lines through a broad range  
 65 of energies was confirmed by in-situ particle and electro-magnetic waves observations [Szalay et al.,  
 66 2018; Sulaiman et al., 2020]. However, a greater surprise came from the finding of protons beams  
 67 and conics, originating from three different regions along the Alfvén wing [Szalay, Allegrini, Bagenal,  
 68 Bolton, Bonfond, Clark, Connerney, Ebert, Gershman, Giles, Gladstone, Greathouse, Hospodarsky,  
 69 Imai, Kurth, Kotsiaros, Louarn, McComas, Saur, Sulaiman and Wilson, 2020; Clark et al., 2020].  
 70 Finally, ion-cyclotron waves and whistler-mode waves excited by the field-aligned electrons are also  
 71 observed [Sulaiman et al., 2020].

72 An important question, however, is whether these phenomena were specific to Io’s case, this  
 73 moon being the most volcanically active body of the solar system and the main source of material  
 74 in the magnetosphere, or whether they could be extended to other moons, such as Europa and  
 75 its induced magnetosphere related to its sub-surface ocean or, and this is the focus of our present  
 76 interest, to Ganymede and its permanent intrinsic magnetic field.

77 Io lacking a permanent magnetic dipole, its non-local interaction with the Jovian magnetic field  
 78 consists of 1) its steady Alfvén wings, which result from the stacking of Jupiter’s magnetic field  
 79 upstream of Io and its subsequent deflection around the satellite [Saur et al., 2004], and 2) a dense  
 80 plasma wake that is rapidly re-accelerated downstream [Hinson et al., 1998].

81 The existence of an intrinsic magnetic field implies some modifications of this picture for  
 82 Ganymede ([Chapter 3.1](#)). The obstacle in Jupiter’s rotating magnetic field is not Ganymede’s body  
 83 or ionosphere but its magnetosphere, of 2–3  $R_G$  radius ( $R_G$  stands for Ganymede’s radius,  $\sim 2634$   
 84 km). The orientation of Ganymede’s internal field, antiparallel to Jupiter’s, leads to a favourable  
 85 orientation of interacting magnetic fields resulting in reconnection at Ganymede’s upstream and  
 86 downstream magnetopause and subsequent particle energization. A signature of this reconnection

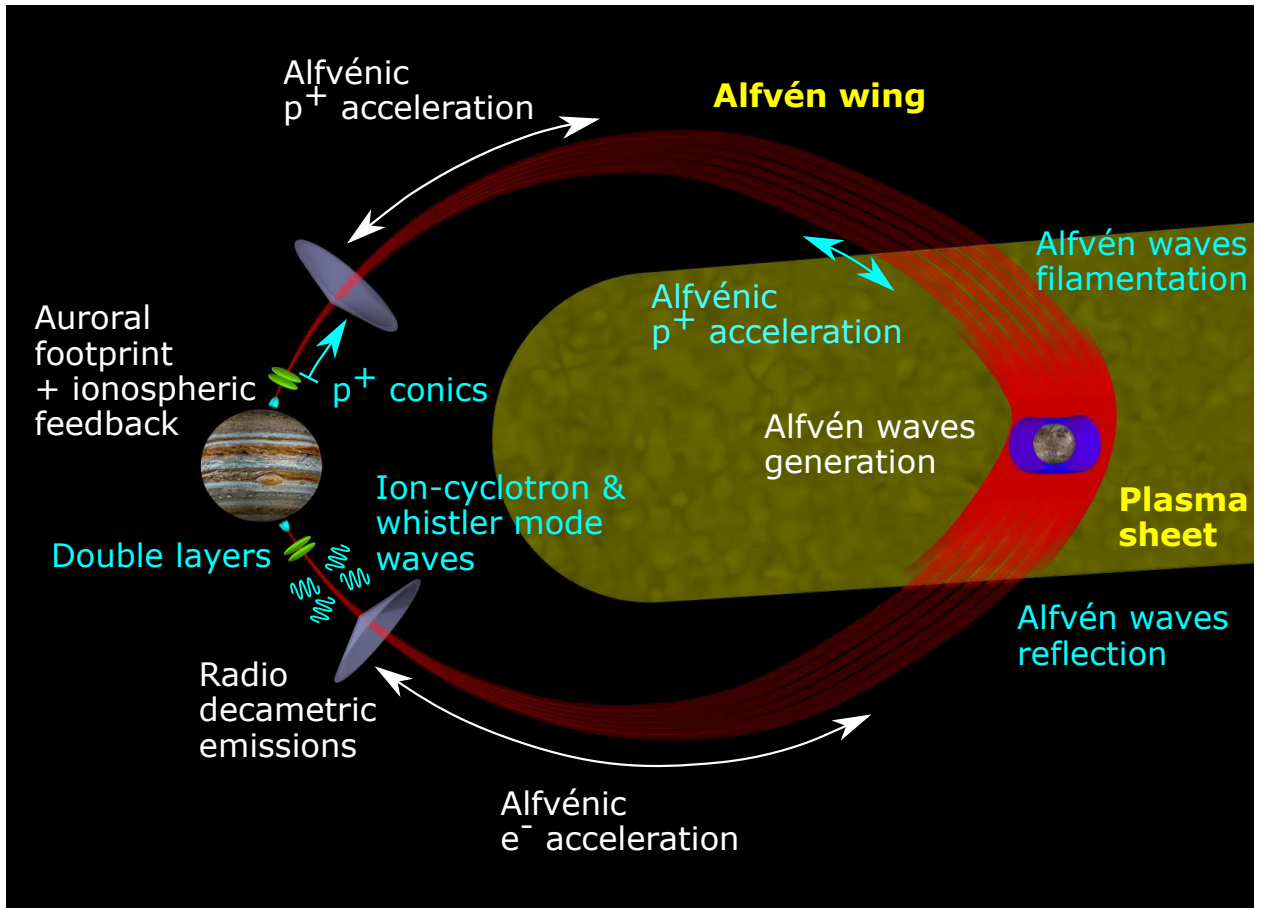


Figure 3.1: Schematic of the chain of processes taking place along the Alfvén wings (in red) generated by the interaction between the magnetosphere of Ganymede (in blue, not to scale) and that of Jupiter. The processes noted in white have already been observed at Ganymede and are the subject of the present chapter while those noted in cyan have not been discovered yet, but are expected to exist because they have already been detected at Io.

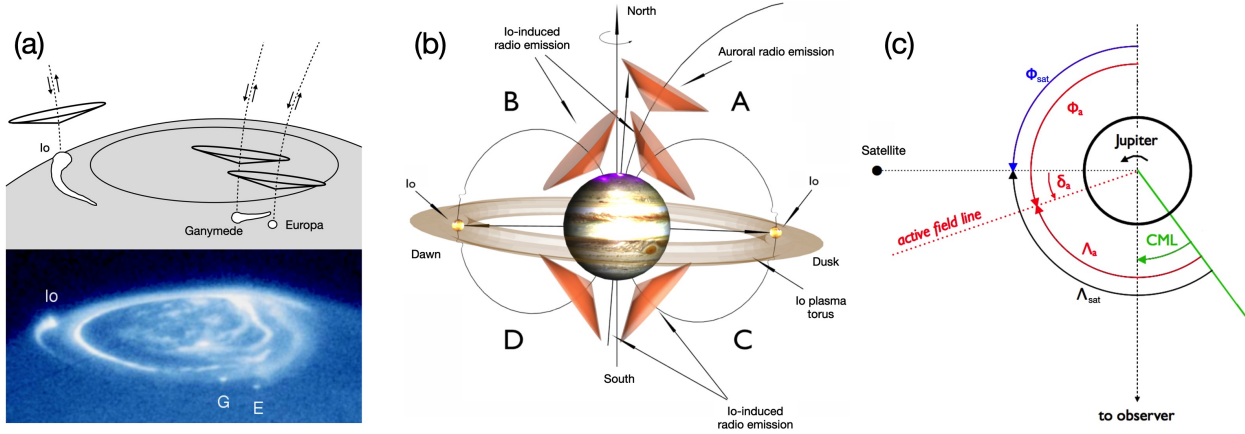


Figure 3.2: (a) Hubble Space Telescope UV image of northern Jovian auroral regions, showing the bright main auroral oval and the footprints of Io (and its tail-like wake-induced emission), Ganymede and Europa flux tubes. In the sketch on the top, hollow conical beams of radio emission are displayed. They are produced above the UV hot spots by the energetic electrons precipitated along the satellite flux tubes or reflected upwards by magnetic mirroring. Similar radio emission originate from sources distributed above the main oval. (b) Geometry and nomenclature of auroral and satellite-induced (here Io-induced) radio emissions. Radio emission is produced along the displayed conical shells, and thus observable only when the source is near a limb of Jupiter. The magnetic field line connected to Io is sketched as the active, radio-emitting field line but actually the active field line leads the instantaneous Io field line by several degrees (angle  $\delta_a$  of panel (c)). (c) Definition of the different angles used to characterize the observing geometry. In green is the central meridian longitude (CML), which is the System III longitude of the observer. The satellite phase  $\Phi_{sat}$  and its System III longitude  $\Lambda_{sat}$  are drawn in blue and black, respectively. Alfvén lead angle  $\delta_a$ , phase, and phase  $\Phi_a$  and longitude  $\Lambda_a$  of the so-called “active” field line (in UV and radio) are shown in red. (a) from Clarke et al. [2002]; Zarka [2007], (b & c) from Marques et al. [2017].

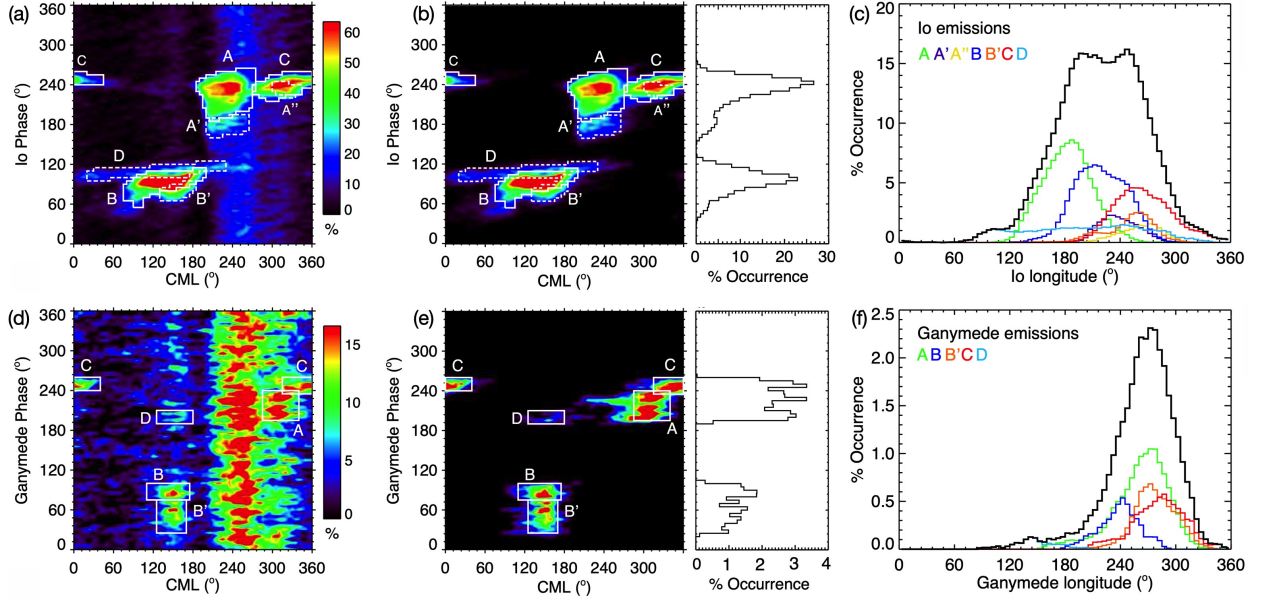


Figure 3.3: (a) Occurrence probability of Jovian radio emissions detected over 26 years (1990–2015) with the Nançay Decameter Array, displayed as 2D histograms as a function of planetary rotation (CML) and Io’s orbital phase ( $\Phi_{Io}$ ) in  $5^\circ \times 5^\circ$  bins (smoothed via  $1^\circ$  interpolation). Regions of high occurrence labelled in white correspond to Io–Jupiter emissions (named Io-A, Io-B...). Vertical bands of emission covering restricted CML ranges at all  $\Phi_{Io}$  correspond to non-Io emissions (auroral or induced by other satellites). (b) Occurrence probability of Io–Jupiter emissions only vs. CML and  $\Phi_{Io}$ . The profile integrated over all CML is displayed on the right side panel. (c) Integrated occurrence probability of Io–Jupiter emissions vs. Io’s Jovicentric longitude ( $\Lambda_{Io} = CML + 180^\circ - \Phi_{Io}$ ). Components from panel (b) are identified by colours, and their sum is the black line. (d) Occurrence probability of non-Io emissions vs. CML and Ganymede’s orbital phase  $\Phi_{Ganymede}$ . Ganymede–Jupiter emissions show up within new regions of enhanced occurrence (white boxes), labelled A–D in reference to the non-Io components in which they have been identified. (e) Occurrence probability of Ganymede–Jupiter emissions only, vs. CML and  $\Phi_{Ganymede}$ . The profile integrated over all CML is displayed on the right side panel. (f) Integrated occurrence probability of Ganymede–Jupiter emissions vs. Ganymede’s jovicentric longitude ( $\Lambda_{Ganymede} = CML + 180^\circ - \Phi_{Ganymede}$ ). Components from panel (e) are identified by colours, and their sum is the black line. From Zarka et al. [2018].

87 is the double loss-cone distributions (i.e. in both directions along the field line) observed by Galileo  
 88 on magnetic field lines connected to both Ganymede and Jupiter [Williams et al., 1997]. At high  
 89 energies (keV — tens of keV), particles can bounce several times between mirror points close to  
 90 Ganymede and close to Jupiter before the magnetic field line drifts across Ganymede’s magne-  
 91 sphere, and then be temporarily trapped and exhibit double loss-cone distributions whereas at low  
 92 energies, the larger pitch angle diffusion fills the loss-cones at some distance from the mirror points  
 93 [Williams and Mauk, 1997].

94 The plasma energized by magnetic reconnection at the magnetopause also generate local electro-  
 95 static and electromagnetic emissions [Gurnett et al., 1996; Kurth et al., 2000], much more developed  
 96 than at Io, described in [Chapter 3.1](#).

97 Beyond a few  $R_G$  downstream of Ganymede, one finds Alfvén wings similar to Io’s [Jia et al.,  
 98 2008] as well as an extended plasma wake [Kivelson et al., 1998]. The Alfvén wings carry a current  
 99 about 0.5 MA [Lavrukhin and Alexeev, 2015] driven by a transverse electric potential drop of about  
 100 80 kV across Ganymede’s magnetosphere [Zhou et al., 2020] (versus a current  $\sim 1$  MA driven by  
 101 a 400 kV potential drop across Io’s ionosphere). The Alfvén wings field-aligned currents close in  
 102 Ganymede’s and Jupiter’s ionospheres and in Ganymede’s magnetotail or plasma wake [Jia et al.,  
 103 2008].

104 For Solar wind–planet interactions, the energy release is often sporadic (substorms) as a result  
 105 of the variable character of the Solar wind and of magnetic flux storage in the magnetotail. But  
 106 at Ganymede, immersed in Jupiter’s magnetosphere, the upstream magnetic field conditions are  
 107 essentially steady, with a slowly rocking orientation of the magnetic field external to Ganymede’s  
 108 magnetosphere. As a consequence, steady reconnection was anticipated at Ganymede’s magne-  
 109 topause, not bursty, substorm-like one [Kivelson et al., 2004]. These expectations were challenged  
 110 by the reanalysis of Galileo plasma data recorded near Ganymede, showing plasma flows accel-  
 111 erated by time-variable magnetic reconnection consistent with Dungey-type substorms [Collinson  
 112 et al., 2018].

113 Another source of variability of the interaction comes from the fact that Ganymede does not  
 114 orbit permanently in a dense plasma environment like Io in its torus, but it periodically crosses the  
 115 Jovian plasma sheet. Its plasma environment is thus very variable, and induces a variable travel  
 116 time of the Alfvénic perturbations between Ganymede and Jupiter. Bonfond et al. [2013] found a  
 117 maximum longitudinal shift of  $13^\circ$  between the multiple spots of the Ganymede northern UV auroral  
 118 footprint and Ganymede’s instantaneous longitude, quite comparable to Io’s lead angle up to  $\sim 15^\circ$

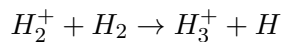
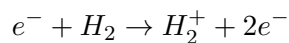
119 in the North and  $\sim 8^\circ$  in the South [Bonfond, Saur, Grodent, Badman, Bisikalo, Shematovich,  
120 Gérard and Radioti, 2017; Hinton et al., 2019].

### 121 **3.6.2 Auroral footprints**

#### 122 **Discovery of the Ganymede footprint**

123 While the first detection of a satellite auroral footprint, Io's, took place in the infrared domain from  
124 a ground based telescope [Connerney et al., 1993], all the subsequent first detections happened in  
125 the ultraviolet (UV) domain. The Europa and Ganymede footprints were first discovered with the  
126 Hubble Space Telescope (HST) [Clarke et al., 2002]. Then came the discovery of the Enceladus  
127 footprint with the Ultraviolet Imaging Spectrograph (UVIS) on board Cassini [Pryor et al., 2011].  
128 Finally, a tentative identification of a Callisto footprint was reported, based on HST UV images  
129 as well [Bhattacharyya et al., 2018]. The Ganymede and Europa footprints have since also been  
130 identified in the infrared domain around  $3.4 \mu m$  with the Jupiter InfraRed Auroral Mapper (JIRAM)  
131 camera on board Juno [Mura et al., 2017].

$H$  and  $H_2$  UV auroral emissions on one hand, and  $H_3^+$  infrared emissions on the other hand,  
both arise from the precipitation of charged particles into Jupiter's  $H$  and  $H_2$  atmosphere. The UV  
emissions result from the de-excitation of atomic or molecular hydrogen after impact by precipitat-  
ing particles (electrons or ions) or secondary electrons. Conversely, auroral infrared emissions are  
thermal emissions of  $H_3^+$  ions which are themselves an indirect product of the electron precipitation  
followed by charge transfer [see review in Badman et al., 2015]:



132  $H_3^+$  emissions are usually observed around  $3.4 \mu m$  because the strong absorption from  $CH_4$  molecules  
133 located at lower altitude than most of the aurora offer a high contrast between the auroral emissions  
134 and the planetary background at this wavelength.

#### 135 **Morphology of the Ganymede footprint**

136 The first detections only associated one auroral spot with the Ganymede footprint [Clarke et al.,  
137 2002]. On HST images, this spot can be fitted with an ellipse of area  $\sim 5 \times 10^5 km^2$ . When mapped  
138 back into the equatorial plane along magnetic field lines, such a surface corresponds to a disk with



139 8-20 times Ganymede's radius ( $R_G = 2634$  km), thus corresponding to the size of Ganymede's  
 140 magnetosphere, rather than Ganymede itself [Grodent et al., 2009].

141 Using their characteristic motion on polar projections fixed in System III (the longitude system  
 142 fixed with the magnetic field), it was found that, in some cases, at least two spots could be associated  
 143 with the footprint of Ganymede [Bonfond et al., 2013] (Figure 3.4). The spacing between these two  
 144 spots increases up to a maximum of about 4000 km and then decreases systematically as a function  
 145 of the position of Ganymede with respect to the plasma sheet, and they seem to merge when  
 146 Ganymede is close to the central region of the sheet. This evolution of the inter-spot distances  
 147 suggests that one spot corresponds to the main Alfvén wing (MAW) and the second one to the  
 148 trans-hemispheric electron beam (TEB), i.e. generated by electrons accelerated in the opposite  
 149 hemisphere (see Figure 3.4 b).

150 The inter-spot distance also varies on timescales larger than Jupiter's rotation. Observations  
 151 carried out in 2007 in similar Ganymede longitude ranges, but a few weeks apart, showed that  
 152 this distance can vary by a factor of 2. Since the distance between spots is directly related to the  
 153 Alfvén propagation time, such variations were attributed to an increase of plasma density in the  
 154 Jovian magnetosphere that took place in the first month of 2007 [Bonfond et al., 2013]. Indeed,  
 155 several other observations, such as the brightening of Jupiter's sodium nebula [Yoneda et al., 2009],  
 156 the decrease of the hectometric (HOM) radio emissions unrelated to the solar wind fluctuations  
 157 [Yoneda et al., 2013], the increased occurrence rate of large plasma injection auroral signatures and  
 158 the expansion of the main auroral oval over 3 months [Bonfond et al., 2012] all indirectly suggest  
 159 that the plasma input from Io increased from February to June 2007.

160 In addition to the spots, an extended auroral tail ( $\geq 24^\circ$ ) can also sometimes be seen in the  
 161 downstream direction along the Ganymede footpath [Bonfond, Saur, Grodent, Badman, Bisikalo,  
 162 Shematovich, Gérard and Radioti, 2017]. As for many features of the Ganymede footprint, this tail  
 163 is harder to detect in UV images than Io's footprint tail. Moreover, even in similar geometrical  
 164 configurations, the Ganymede footprint UV tail has only been identified in a handful of cases.  
 165 These rare detections indicate that parameters other than just the position of Ganymede in the  
 166 plasma sheet and the viewing geometry impact its apparent brightness (such as the plasma energy  
 167 distribution, composition, density, the magnetic field strength, etc.). However, the existence of  
 168 tails both in Ganymede's and Europa's footprints indicates that lessons learned from Io's footprint  
 169 most likely also apply for the others and vice-versa. Two main ideas have been proposed to explain  
 170 the Io footprint tail. The first one involves a steady current loop related to the reacceleration

171 of the stagnant plasma in Io's wake [Hill and Vasyliunas, 2002; Delamere et al., 2003; Su et al.,  
 172 2003; Ergun et al., 2006; Matsuda et al., 2012], while the second involves the increasingly intricate  
 173 reflection pattern of the Alfvén waves downstream of the satellite [Jacobsen et al., 2007; Bonfond,  
 174 Saur, Grodent, Badman, Bisikalo, Shematovich, Gérard and Radioti, 2017]. The broad energy  
 175 distribution inferred from remote observations [Bonfond et al., 2009] and observed directly by Juno  
 176 favour the second [Szalay et al., 2018]. It is this noteworthy that the existence of a footprint tail  
 177 at Ganymede, where no significance mass loading takes place, indicates that this process is not a  
 178 necessary ingredient to the formation of the tail.

179 Infrared observations from the JIRAM instrument on board Juno offer an unprecedented spatial  
 180 resolution, down to 15 km/pixel [Mura et al., 2018; Moirano et al., 2021]. They not only showed  
 181 similar features in infrared  $H_3^+$  emissions than in the UV, such as the pair of spots followed by the  
 182 extended tail [Mura et al., 2017], but they also unveiled further details of the footprint morphology.  
 183 In particular, and similarly to the Io footprint spots, each one of the two Ganymede footprint spots,  
 184 appears to be formed of a pair of smaller auroral dots separated by 170 km (Figure 3.4c) [Mura et al.,  
 185 2018]. One possible explanation is that these dots correspond to the front and tail of Ganymede's  
 186 magnetosphere, where magnetic reconnection takes place. However, the presence of similar sub-  
 187 structures at Io's footprint rather suggests another (and not mutually exclusive) origin, possibly  
 188 related to Jupiter's ionosphere or to the electron acceleration process. This conclusion is further  
 189 strengthened by the finding that the Ganymede footprint tail (as well as Io's and Europa's) was  
 190 also made of sub-dots separated by  $\sim 270$  km (Figure 3.4d). Contrary to the larger spots discussed  
 191 above, these sub-dots appear fixed with the planet rather than following the motion of the satellite  
 192 [Moirano et al., 2021]. Because of this this behaviour, as well as the size and spacing of the spots,  
 193 Moirano et al. [2021] suggest that these features result from the ionosphere feedback instability,  
 194 in which a localized increase of ionospheric conductivity in the presence of background ionospheric  
 195 electric field enhances the ionospheric currents. In this scenario, the current enhancement close  
 196 through field aligned currents at the conductivity gradient through secondary Alfvén waves, which  
 197 further increases the precipitating electron flux and the conductivity, closing the feedback loop.

### 198 **The brightness of the Ganymede footprint**

199 On HST UV images acquired at slant angle, the brightness of the Ganymede footprint can reach  
 200 up to 180 kR [Wannawichian et al., 2010]. The total power emitted by the Ganymede footprint's  
 201 main spot typically ranges between 1 and 6 GW in the  $H_2$  UV Lyman and Werner bands. However,

202 depending on the auroral background emissions, it can also become so dim that it is no longer  
203 identifiable [Bonfond, Grodent, Badman, Saur, Gérard and Radioti, 2017]. The precipitated energy  
204 is approximately 10 times higher than the energy of the resulting UV emissions [Gustin et al.,  
205 2012]. Assuming that 10 % of the Poynting flux carried by the Alfvén waves is converted into  
206 electron acceleration, this emitted UV power is in highest part or slightly higher than the range  
207 predicted by the models of satellite-magnetosphere interaction [Saur et al., 2013]. Because the  
208 moon-magnetosphere interaction depends on the local plasma density, the emitted power is the  
209 highest when Ganymede is in the center of the plasma sheet and decreases outside of it [Grodent  
210 et al., 2009]. However, it also varies at two shorter timescales: in the range of 10-40 minutes and  
211 in the range of 2-3 minutes. The first one probably corresponds to Ganymede’s traversal time of  
212 plasma bubbles with properties differing from the surrounding environment, such as the plasma  
213 injections typically observed at such radial distances [Mauk et al., 1997]. A detailed analysis of  
214 some HST sequences showed the Ganymede footprint disappearing as it was traversing the auroral  
215 signature of such a plasma injection, further adding confidence into this explanation [Bonfond,  
216 Grodent, Badman, Saur, Gérard and Radioti, 2017]. A similar behavior had already been reported  
217 for the Io footprint [Bonfond et al., 2012] and Hess, Bonfond and Delamere [2013] argued that  
218 this disappearance was most probably due to the increased electron density at high latitude which  
219 limited the efficiency of the parallel electron acceleration by inertial Alfvén waves. The 2-3 minutes  
220 timescale could either be related to the recurrence time of bursty magnetic reconnection at the  
221 front of Ganymede’s magnetosphere, in accordance with the MHD simulations [Jia et al., 2008;  
222 Zhou et al., 2019, 2020], or to the quasi-periodic formation, upward migration and disappearance  
223 electric potential drops of a few hundred Volts at altitudes around  $0.2 R_J$  above Jupiter’s surface.  
224 The latter scenario, which is not mutually exclusive with the first one, is proposed in analogy with  
225 similar structures found at the Io footprint from observations of fast-drifting radio S-bursts [Hess  
226 et al., 2009], and could explain the 2-3 minutes fluctuations of the UV brightness of the Io, Europa  
227 and Ganymede footprints [Bonfond et al., 2007; Grodent et al., 2009; Bonfond, Grodent, Badman,  
228 Saur, Gérard and Radioti, 2017].

### 229 **3.6.3 Radio emissions**

#### 230 **Induced radio emissions**

231 The electrons accelerated in the Alfvén wings to energies of a few keV to tens of keV give rise, close  
 232 to Jupiter, to intense radio emission via the Cyclotron Maser Instability (CMI) mechanism [Zarka,  
 233 1998; Hess, Mottez and Zarka, 2007; Hess et al., 2008]. The emission is produced close to the local  
 234 electron cyclotron frequency, that can reach 40 MHz in Jupiter’s ionosphere [Connerney et al., 2018],  
 235 and it is beamed at large angle from the magnetic field in the source (Figures 3.2a,b). The part  
 236 above 10 MHz (corresponding to the decametre – DAM — wavelength range) can propagate through  
 237 the Earth’s ionosphere and be detected by ground-based antenna arrays, as done by Bigg [1964] and  
 238 others (e.g. [Lamy et al., 2017]). Accumulated observations revealed for the Io–Jupiter interaction  
 239 four islands of enhanced emission occurrence in the  $\Phi_{Io}$ –CML (Central Meridian Longitude =  
 240 observer’s Jovian System III longitude) plane (Figure 3.3a,b). Those correspond to two physical  
 241 sources, near both Io Flux Tube (IFT) northern and southern footprints, seen on the eastern and  
 242 western limbs of the planet because CMI emission is beamed nearly perpendicular to the IFT field  
 243 lines [Marques et al., 2017] (Figure 3.2b). The high occurrence islands are not symmetrical around  
 244  $\Phi_{Io} = 180^\circ$  due to Alfvén wave propagation through Io’s torus to Jupiter’s ionosphere, that induces  
 245 a time-variable angular shift (so-called lead angle) that depends on the position of Io in the plasma  
 246 torus (Figures 3.2c).

#### 247 **Radio searches**

248 The result from Bigg [1964] demonstrated that existence of a satellite-induced radio emission could  
 249 be statistically established by building emission occurrence versus the satellite phase  $\Phi$ , or in the  
 250  $\Phi$ –CML plane. Many observers subsequently searched for the statistical evidence of the interaction  
 251 of Jupiter’s magnetic field with the other Galilean moons plus Amalthea via ground-based DAM  
 252 observations  $\geq 10$  MHz, at the Universities of Florida, Chile (narrow-band observations distributed  
 253 between 15 and 28 MHz), and Colorado (swept-frequency spectrograph 7.6–41 MHz). Lebo et al.  
 254 [1965] and Bigg [1966] mentioned marginal effects of Europa and Ganymede, but those were not  
 255 confirmed by subsequent studies involving up to 18 years of accumulated observations (1957–75),  
 256 that found no other effect than Io’s [Dulk, 1967; Kaiser and Alexander, 1973; St. Cyr, 1985].  
 257 The instruments used had low sensitivity (minimum detectable flux density  $\sim 10^4$  Jy =  $10^{-22}$   
 258  $Wm^{-2}Hz^{-1}$ ).

259 The Galileo plasma wave instrument provided several years of continuous observations (1995-  
 260 2002) in the hectometre range (2.1–5.6 MHz), that were statistically analysed in the same way.  
 261 Low significance occurrence peaks were found in the  $\Phi_{Ganymede}$ -CML plane by Menietti, Gurnett,  
 262 Kurth and Groene [1998]. Including 10 months of Cassini observations, Hospodarsky et al. [2001]  
 263 found a similar result as well as a marginal dependence on  $\Phi_{Callisto}$ . Higgins [2007] obtained analog  
 264 results from the analysis of Voyager 1 and 2 data in the range 2.1–5.8 MHz. Besides these statistical  
 265 studies, radio emission induced by Ganymede was tentatively identified through an occultation by  
 266 Ganymede’s body itself [Kurth, Bolton, Gurnett and Levin, 1997] and radio direction-finding by  
 267 Galileo [Menietti, Gurnett, Kurth, Groene and Granroth, 1998], and it was proposed as the possible  
 268 source of rare circular patches observed in Ulysses radio dynamic spectra [Kaiser and MacDowall,  
 269 1998]. But none of these interpretations was unique, and hence convincing.

270 Radio emissions produced by Ganymede’s magnetosphere itself were also discovered at low  
 271 frequencies ( $\leq 100$  kHz) by Galileo [Gurnett et al., 1996; Kurth, Gurnett, Roux and Bolton, 1997]  
 272 (see also [Chapter 3.1](#)). These local radio emissions are not generated by the CMI, due to a  $f_{pe}/f_{ce}$   
 273 ratio  $> 0.3$  close to Ganymede, too high for the CMI to develop, but by conversion of electrostatic  
 274 waves.

## 275 Radio detections

276 Three recent studies detected independently and unambiguously the DAM emissions induced by  
 277 Ganymede in Jupiter’s magnetic field.

278 Louis, Lamy, Zarka, Cecconi and Hess [2017] was based on simulations by the ExpRES code  
 279 (published in [Louis et al., 2019]). This code, based on CMI physics, predicts the shape of radio  
 280 arcs in the time-frequency plane for a selected observer’s position or trajectory relative to Jupiter.  
 281 For satellite–Jupiter interactions, that results in an “active” magnetic flux tube (where electron  
 282 acceleration takes place – Figure 3.2c) and thus a radio source of limited size, the predicted arcs are  
 283 well defined and locally isolated in the time-frequency plane, rather than being drowned in series  
 284 of nested arcs as is the case for auroral DAM (Figure 3.5). ExpRES simulations were compared  
 285 to Voyager and Cassini radio observations in [Louis, Lamy, Zarka, Cecconi and Hess, 2017; Louis,  
 286 Lamy, Zarka, Cecconi, Hess and Bonnin, 2017], leading to the identification of  $\sim 100$  Ganymede–  
 287 Jupiter radio arcs around  $\Phi_{Ganymede} \sim 100^\circ$  and  $260^\circ$ , in broad CML ranges. These ranges of  
 288  $\Phi_{Ganymede}$  and CML correspond to Ganymede’s Jovian longitude of  $\Lambda_{Ganymede} = 160^\circ - 300^\circ$  in  
 289 the northern hemisphere and  $\Lambda_{Ganymede} = 0^\circ - 100^\circ$  in the southern hemisphere ( $\Lambda_{Ganymede} =$

290  $CML + 180^\circ - \Phi_{Ganymede}$ ). Radio arcs cover the spectral ranges  $\sim 1$ -30 MHz in the north and  
 291  $\sim 1$ -16 MHz in the south. Their duration is  $\sim 40$ -60 minutes. The typical energy of the electrons in  
 292 EXPRES simulations matching the observations is a few keV.

293 Zarka et al. [2018] performed a statistical study similar to those of the earlier radio searches  
 294 described above, but this time applied to a much longer database, consisting of 26 years of daily  
 295 observations of Jupiter with the Nançay Decameter Array in the range 10-40 MHz, with a sensitivity  
 296  $\sim 1.5 \times 10^3$  Jy, i.e.  $\sim 7$  times better than earlier observations [Marques et al., 2017]. With this  
 297 database, islands of enhanced occurrence clearly showed up in the  $\Phi_{Ganymede}$ -CML plane (Figures  
 298 3.3d,e), with a signal-to-noise ratio of up to  $13\sigma$ . These islands, strongly reminiscent of Io-Jupiter  
 299 ones, cover the ranges of Ganymede phases  $65^\circ \pm 40^\circ$  and  $225^\circ \pm 35^\circ$  at CML around  $155^\circ$  and  
 300  $310^\circ$  respectively, and gather 360 Ganymede-Jupiter emissions. They correspond to a range of  
 301 Ganymede's longitude  $220^\circ \pm 50^\circ$  (Figure 3.3f), very similar to the range of Io's longitudes for which  
 302 Io-DAM emission is detected (Figure 3.3c). Northern emissions reach 33 MHz and southern ones 27  
 303 MHz. The difference in the CML and  $\Phi_{Ganymede}$  ranges found by Louis, Lamy, Zarka, Cecconi and  
 304 Hess [2017] can be explained by the different spectral ranges covered by the observations and by the  
 305 slightly different Jovian latitudes of the observers. The fact that Ganymede-Jupiter emissions do  
 306 not reach frequencies as high as the Io-Jupiter ones ( $\sim 40$  MHz) is due to the fact that the northern  
 307 footprint of the Ganymede flux tube (latitude  $\sim 75^\circ$ ) lies northward of the northern high-amplitude  
 308 magnetic anomaly at the surface of Jupiter crossed by the northern Io flux tube footprint (latitude  
 309  $\sim 66^\circ$ ), implying that lower electron cyclotron frequencies are reached at Ganymede's flux tube  
 310 footprint.

311 The third study is the in-situ exploration by Juno of Ganymede's wake, described in the next  
 312 section.

### 313 3.6.4 In situ observations associated with the Ganymede footprint

314 Juno's orbit and instruments' suite are particularly well suited to combine remote sensing observa-  
 315 tions of the auroral emissions and in situ measurements of the particles and waves giving rise to these  
 316 emissions. In particular, on 29 May 2019, during Juno's 20th perijove operations, between 07:37:14  
 317 and 07:37:32, the spacecraft crossed Ganymede's footpath (i.e. the mapping of Ganymede's orbit  
 318 along the magnetic field lines) only  $8^\circ$  downstream of the footprint's main spot, as observed from the  
 319 Juno UltraViolet Spectrograph (Juno-UVS). All in situ instruments showed clear signatures of the  
 320 crossing [Szalay, Allegrini, Bagenal, Bolton, Bonfond, Clark, Connerney, Ebert, Gershman, Giles,

321 Gladstone, Greathouse, Hospodarsky, Imai, Kurth, Kotsiaros, Louarn, McComas, Saur, Sulaiman  
 322 and Wilson, 2020]. For example, the magnetometer data recorded evidence of both significant field-  
 323 aligned currents (in the form of deviations of the azimuthal magnetic field component  $\delta B_\phi$ ) and  
 324 strong Alfvénic activity with Poynting fluxes  $\sim 100 \text{ mW/m}^2$  (see Figure 3.6(d)). On the other hand,  
 325 the JADE (Jovian Auroral Distributions Experiment) particle instrument recorded field-aligned en-  
 326 hancement of the electron flux in both directions (see Figure 3.6(a), (b) and (c)). The precipitating  
 327 electrons energy flux reached  $11 \text{ mW/m}^2$ , which is  $\sim 10\%$  of the Poynting energy flux. The electron  
 328 energy distribution did not show a peaked feature, which would be expected from acceleration by  
 329 a discrete quasi-static electric field, but a broadband enhancement in the range from 0.5 to 40 keV,  
 330 compatible with an Alfvénic acceleration process.

331 From the crossing time, the inferred width of the whole footprint tail is 660 km, however, the  
 332 current system is highly structured, and smaller scale ( $\sim 50\text{km}$ ) sub-structures also apparent in the  
 333 JADE data as well. Moreover, the pitch angle distribution shows that the electron acceleration is bi-  
 334 directional since a significant flux of up-going electrons was observed. Finally, JADE measurements  
 335 also revealed upward electron conics in downward currents, which further bolsters the explanation  
 336 involving particle acceleration by inertial Alfvén waves near the Jovian ionosphere. These findings,  
 337 as well as the discovery of a similar accelerated broadband electron distribution in the Europa  
 338 footprint tail [Allegrini et al., 2020], further strengthens the idea that similar processes are at play  
 339 for all footprints.

340 During the same event, Juno also crossed the source region of the decametric radio emissions  
 341 related to the Ganymede footprint tail [Louis et al., 2020].

342 Measurements by Juno/Waves and JADE showed that these decametric emissions are produced  
 343 slightly (0.5–2.1%) above the local  $f_{ce}$  and beamed at  $76^\circ$  to  $83^\circ$  from the magnetic field. These  
 344 results are fully consistent with their generation by the loss-cone driven CMI (as opposed to a shell-  
 345 driven one that would generate perpendicular waves). The electrons triggering these emissions,  
 346 likely accelerated by Alfvén waves, have an energy of 4-15 keV. The size of the radio source region  
 347 was at least  $250 \pm 50 \text{ km}$  wide perpendicular to the magnetic field (it is spread along thousands of  
 348 km along the field lines, different frequencies being emitted at different altitudes, where  $f \sim f_{ce}$  ;  
 349 as a rule of thumb, 1 kHz bandwidth corresponds to  $\sim 1 \text{ km}$  extent along Jovian high latitude field  
 350 lines).

### 351 **3.6.5 What electromagnetic emissions from satellite footprints teach us on mag-** 352 **netospheric physics**

#### 353 **The Ganymede footprint as a landmark in the Jovian magnetosphere**

354 The satellite footprints are extremely valuable landmarks in the aurora, as they directly connect via  
355 magnetic field lines the associated moons at their orbital distance to their ionospheric conjugates.  
356 The location of the Io footprint has thus been used as a constraint to increase the accuracy of the  
357 internal magnetic field models. For example, the VIP4 (Voyager, Io, Pioneer, 4th order) magnetic  
358 field model uses infrared observations of the Io footpath location to complement the in-situ magnetic  
359 measurements from the Pioneer and Voyager spacecraft and increase the model accuracy in the  
360 polar regions [Connerney et al., 1998]. However, an analysis of the footpaths of Io, Europa and  
361 Ganymede based on HST UV observations in the northern hemisphere showed that the three con-  
362 tours diverge in the region centered around  $100^\circ$  System III longitude [Grodent, Bonfond, Gérard,  
363 Radioti, Gustin, Clarke, Nichols and Connerney, 2008]. The peculiar shape of the different foot-  
364 paths could be reproduced by adding a small localized dipole magnetic field to the global multipolar  
365 magnetic field model, interpreted as indicative of a localized magnetic anomaly. The VIPAL (Voy-  
366 ager, Io, Pioneer, Anomaly, Longitudes) model was based on a larger set of UV observations, using  
367 both the latitude and the longitude of the Io's footprint main spot (rather than just the footpath  
368 location), to improve the model's accuracy, especially in the magnetic anomaly region [Hess and  
369 Delamere, 2012]. Finally, the ISaAC (In Situ and Auroral Constrains) model [Hess et al., 2017] used  
370 the same technique, but also accounting for the location of the Europa and Ganymede footprints to  
371 further refine the model. In the polar regions, the result was indeed remarkably close to the later  
372 results from the JRM09 model, which is derived solely from the highly accurate magnetic field mea-  
373 surements from Juno's first 9 orbits [Connerney et al., 2018]. Juno's measurements also confirmed  
374 the presence and location of the magnetic anomaly in the northern polar region. It should however  
375 be noted that only Juno's measurements could identify the larger magnetic anomaly often named  
376 the "Big Blue Spot", which is located much closer to the equator [Moore et al., 2017; Connerney  
377 et al., 2018], where footprints locations provide no useful constrains.

378 The size of the contour of the main auroral emissions at Jupiter can change from one Jovian  
379 rotation to another, superimposed to long term trends over a few months [Bonfond et al., 2012].  
380 It is however challenging to infer whether these changes are related to variations of the radial  
381 distance from which these aurora originate, or to the variable stretching of the magnetic field



382 lines. At Ganymede’s distance from Jupiter, the influence on the mapping of the current sheet’s  
 383 magnetic field, which distorts the magnetic field radially, is much larger than at Io’s. Grodent,  
 384 Gérard, Radioti, Bonfond and Saglam [2008] indeed noted that, while the location of the Io footpath  
 385 remained remarkably stable through time, the magnetic latitude of the Ganymede footpath could  
 386 move by as much as  $2.4^\circ$  and the main emissions by  $\sim 3^\circ$ . Such a shift could be reproduced by  
 387 modifying the current sheet thickness from  $5R_J$  to  $2.5R_J$  in the VIP4 model [Connerney et al.,  
 388 1998], which uses the current sheet model of Connerney [1981]. Moreover, on at least one occasion,  
 389 the Ganymede footprint was seen inside the main emissions instead of outside [Bonfond et al., 2012].  
 390 Not only did the main emissions expand equatorward down to Ganymede, but the the Ganymede  
 391 footprint itself had moved out by  $0.5^\circ$ . This unique observation indicated that both the stretching  
 392 of the magnetic field lines and the radial distance of the of the region mapping to the main emissions  
 393 can change through time.

394 Finally, magnetic field models based on multi-polar developments of the internal field and an  
 395 axisymmetric representation of the current sheet, such as VIP4, VIPAL, ISaAC or JRM09, are in-  
 396 creasingly inaccurate beyond  $30 R_J$ . In particular, local time effects become increasingly important  
 397 beyond this distance [Khurana, 1997]. An alternative method to field tracing models is based on  
 398 the flux equivalence principle [Vogt et al., 2011, 2015]. Starting from a distance where the mapping  
 399 is known, the iterative construction of this mapping model consists of finding the ionospheric coun-  
 400 terpart of an a elemental area in the equatorial magnetosphere by equating the magnetic flux in  
 401 the two regions. Again, the footpath of Ganymede serves as a reliable reference point, from which  
 402 contours at increasingly large distances in the magnetosphere are progressively mapped into the  
 403 ionosphere.

#### 404 **Radio emissions durations**

405 The duration of Io–Jupiter DAM emissions was found to be statistically twice that of auroral DAM  
 406 emissions [Marques et al., 2017; Zarka et al., 2018]. This can be understood because auroral DAM  
 407 is controlled by Jupiter’s rotation of period  $\sim 10$ h whereas Io–Jupiter DAM is primarily controlled  
 408 by Io’s orbital motion of period  $\sim 42$ h, combined with a narrow radio beaming and from a steady  
 409 Alfvén wings system fixed (at first order) relative to Io. Ganymede’s orbital period being four times  
 410 that of Io, one might have expected, in the case of steady magnetic reconnection and Alfvén wings  
 411 attached to that moon, a duration of Ganymede–Jupiter DAM emissions statistically longer than  
 412 for Io. Zarka et al. [2018] developed a method for comparing the broad distributions of durations of

413 these radio emission, and not only their moments. They showed that the duration of Ganymede–  
 414 induced DAM radio bursts, between  $\sim 10$  min. and  $\sim 3\text{h}30$ , was statistically 1.7 times shorter than  
 415 that of Io–Jupiter ones, and only  $\sim 1.2$  times longer than auroral DAM bursts. This implies that  
 416 Ganymede–Jupiter interaction is dominated by Jupiter’s rotation.

417 One possible explanation is that the efficiency of the reconnection between Jupiter and Ganymede  
 418 magnetic fields varies with Jupiter’s rotation. Analysing an analytical criterion for reconnection  
 419 onset, Kaweeyanun et al. [2020] found that reconnection may occur anywhere on Ganymede’s mag-  
 420 netopause in an unpredictable, disordered way, the average reconnection rate being controlled by  
 421 the ambient Jovian field orientation and hence driven by Jupiter’s rotation. MHD simulations [Jia  
 422 et al., 2009, 2010] and MHD-Hall simulations [Zhou et al., 2019, 2020] also showed that magnetic  
 423 reconnection is intrinsically intermittent, involving flux ropes and flux transfer events at timescales  
 424 down to 10–100 s near the upstream magnetopause, even for constant external conditions. But  
 425 these time scales are much shorter than the duration of Ganymede–induced DAM radio bursts.

426 Another explanation is that the conditions permitting CMI emission at Ganymede’s footprints  
 427 (for example the magnetic field topology favouring the existence of a loss cone) exist in a range of  
 428 longitudes more restricted than for Io. This is indeed what is suggested by Figures 3.3c and 3.3f.  
 429 Combined with the synodic period of Jupiter relative to Ganymede being shorter than the synodic  
 430 period of Jupiter relative to Io, this explains the statistically shorter durations of Ganymede–induced  
 431 radio bursts.

432 This, and the persistence of the UV footprints of Ganymede, suggests that the remote elec-  
 433 trodynamic interaction between Ganymede and the Jovian magnetic field is rather steady, and  
 434 consequently that the electrons responsible for the electromagnetic footprint emissions are likely  
 435 accelerated by Alfvén waves rather than by reconnection.

### 436 **Radio emissions energetics**

437 Kurth et al. [2000] qualitatively compared the strength of the local and distant radio emissions and  
 438 plasma waves at the 4 Galilean moons, noting that it is strongest at Io, and “intermediate” at Europa  
 439 and Ganymede. Zarka [2007] extended this comparison to the powers emitted in UV footprints  
 440 and induced CMI radio emissions, still poorly constrained at that time. Grodent et al. [2009]  
 441 better quantified the power emitted in the UV by Ganymede’s footprint (0.2–1.5 *GW*). Following  
 442 their statistical detection of Ganymede–induced radio emissions, Zarka et al. [2018] measured their  
 443 intensity (marginally lower than Io–induced ones) and their emitted power ( $\sim 15\times$  lower than for

444 Io-induced radio emissions). This strengthened the radio-magnetic scaling law proposed in [Zarka  
 445 et al., 2001; Zarka, 2007] and generalized in Fig. 7 of [Zarka et al., 2018], that relates the emitted  
 446 radio power to the intercepted Poynting flux (or magnetic energy flux) in all interactions involving  
 447 a magnetized plasma flow (sub- or super-Alfvénic) and an obstacle (magnetized or not). According  
 448 to this scaling law, the dissipated electromagnetic power writes in all cases

$$P_{dissipated}(W) \simeq \epsilon(V_{flow}B_{\perp flow}^2/\mu_o)\pi R_{obstacle}^2 \quad (3.1)$$

449 with  $B_{\perp flow}$  the flow's magnetic field component perpendicular to the flow direction in the obstacle's  
 450 frame, and an efficiency  $0 < \epsilon \leq 1$  ( $\epsilon \simeq M_A$ , the Alfvén Mach number, for a sub-Alfvénic flow).  
 451 Following equation 3.1, the dissipated power (from the intercepted Jovian magnetic field) in the  
 452 Alfvén wings is similar for Europa and Ganymede, Europa being closer to Jupiter but Ganymede  
 453 having a much larger cross-section due to its magnetosphere, and about one order of magnitude  
 454 smaller than in Io's Alfvén wings. Furthermore, it was found in [Zarka et al., 2001; Zarka, 2007]  
 455 that the emitted radio power resulting from the flow-obstacle interaction follows the relation

$$P_{radio}(W) \simeq \beta(V_{flow}B_{\perp flow}^2/\mu_o)\pi R_{obstacle}^2 = (\beta/\epsilon)P_{dissipated} \quad (3.2)$$

456 with an efficiency factor  $\beta = 2 - 10 \times 10^{-3}$ . Subsequent works explored the theoretical foundations  
 457 of this radio-magnetic scaling law and found that it only provides order of magnitude estimates (see  
 458 [Zarka, 2020] and references therein), but as it seems to hold over  $>10$  orders of magnitude, it remains  
 459 adapted to predictions and analyses of populations. In particular, the Ganymede–Jupiter interaction  
 460 provides a useful model for studying star-planet plasma interactions in which a magnetized hot  
 461 Jupiter interacts with its magnetized parent star, and also possibly some pulsar-planet interactions.

### 462 3.6.6 Summary and perspectives

#### 463 Summary

464 Thanks to the data collected by Galileo during its 6 close flybys of Ganymede in 1995–2000, as well as  
 465 by HST, Juno and ground-based radio telescopes, the electrodynamic coupling between Ganymede  
 466 and the Jovian ionosphere thus seems to be fairly well described and understood at first order.  
 467 Despite the very different nature of the local interaction close to the satellites, the processes taking  
 468 place further away from them appear common to all moons, suggesting that there is a universal  
 469 physics at play, applicable to other systems as well, even beyond our solar system. Among these  
 470 processes are the prominent role of Alfvén waves, not only to carry the electric current, but also

471 to accelerate the electrons along the field lines in both directions. Another common characteristic  
472 is the presence of short length-scale features and short time-scale variations of the footprints, even  
473 if the characteristics of these behaviours are not yet fully elucidated. Moreover, the characteristics  
474 of the radio decametric emissions both at Io and Ganymede demonstrate the importance of the  
475 cyclotron-maser instability and the power of the decametric emissions at Ganymede helped validate  
476 the scaling law between the emitted radio power and the intercepted Poynting flux. Finally, the  
477 location of the Ganymede auroral footprint has also served as a useful landmark to both constrain  
478 the internal magnetic field models before the arrival of Juno and to map auroral features into the  
479 magnetosphere.

### 480 **Open questions and perspectives**

481 In addition to its use as a reference point in the magnetosphere, a careful analysis of the magnetic  
482 footprint of Ganymede could even help us to get one step further: documenting the changes in the  
483 Jovian magnetosphere. The footprint could be a tool to monitor the state of the magnetosphere, by  
484 studying both the latitudinal position of the spots and their spacing. The first one is related to the  
485 azimuthal currents in the plasma sheet, while the second varies directly with the Alfvén propagation  
486 time, which depends on the plasma density and the magnetic field strength. However, to achieve  
487 such an objective, a calibration of the relationship between auroral and magnetospheric parameters  
488 remains to be performed.

489 The coordinates of the high occurrence islands in the  $\Phi_{Ganymede}$ -CML plane (Figures 3.3d,e),  
490 as well as their extension to nearly all CML and different Ganymede phases at low frequencies  
491 [Louis, Lamy, Zarka, Cecconi and Hess, 2017], remain to be quantitatively explained. Another open  
492 question concerning radio emissions is the existence of Ganymede-induced S-bursts and the spatial  
493 structure of electric fields and electrons acceleration along the Ganymede flux tube (e.g., [Hess,  
494 Zarka and Mottez, 2007; Hess et al., 2009] for Io).

495 It would be interesting to search in radio and UV data direct signatures of the intermittent  
496 reconnection between Jupiter's and Ganymede's magnetic fields, and more broadly to correlate the  
497 occurrence of radio and UV emissions at all time scales. However, this quest will not be simple,  
498 because short-timescale (a few minutes) variations of the footprint brightness, which could result  
499 from those bursty reconnections, have also been identified at Io and Europa, where reconnection is  
500 not expected [Bonfond, Grodent, Badman, Saur, Gérard and Radioti, 2017].

501 These two processes are not mutually exclusive and will thus be difficult to disentangle. Further-

502 more, the sub-structure of the Ganymede footprint spots could also be interpreted as a signature  
503 of the reconnection sites at the front and back of Ganymede’s magnetosphere [Mura et al., 2018].  
504 However, here again, a similar spatial pattern has been also identified at Io’s footprint, which also  
505 calls for a common explanation.

506 Moreover, while many pieces of the scenario proposed to explain the footprint spots multiplicity,  
507 such as the measurements of strong Alfvén waves and bi-directional electron beams with a broad  
508 energy distribution, have been confirmed by in situ measurements, a clear demonstration that the  
509 electrons accelerated away from Jupiter in one hemisphere can actually precipitate in the opposite  
510 one remains to be found.

511 Finally, one of the most unexpected findings of Juno regarding the satellite footprints was the  
512 discovery of proton beams during Io’s Alfvén wings crossings, with three different acceleration  
513 regions identified, at altitudes between 0.9 and 2.5  $R_J$ , at the torus boundary and very close to  
514 Jupiter, at altitudes around 0.16  $R_J$  [Szalay, Bagenal, Allegrini, Bonfond, Clark, Connerney, Crary,  
515 Ebert, Ergun, Gershman, Hinton, Imai, Janser, McComas, Paranicas, Saur, Sulaiman, Thomsen,  
516 Wilson, Bolton and Levin, 2020; Clark et al., 2020]. The two former populations are probably  
517 arising from Alfvénic acceleration while the third possibly stems from interactions with ion-cyclotron  
518 waves [Sulaiman et al., 2020]. The first indications that a similar processes also takes place at  
519 Ganymede need to be confirmed [Szalay, Allegrini, Bagenal, Bolton, Bonfond, Clark, Connerney,  
520 Ebert, Gershman, Giles, Gladstone, Greathouse, Hospodarsky, Imai, Kurth, Kotsiaros, Louarn,  
521 McComas, Saur, Sulaiman and Wilson, 2020]. Similarly, energetic proton depletion found in Io’s  
522 wake [Paranicas et al., 2019] probably have a counterpart at Ganymede, even if they haven’t been  
523 found yet.

524 While the Juno mission is essentially dedicated to Jupiter itself, the European JUper ICy  
525 moons Explorer (JUICE) mission, to be launched in mid-2022, will further investigate Ganymede  
526 and its surrounding space environment [Grasset et al., 2013]. After a first phase of the mission  
527 orbiting around Jupiter and flying by Europa, Ganymede and Callisto, the spacecraft is planned to  
528 insert into Ganymede’s orbit. This mission profile will allow to connect directly for the first time  
529 in situ measurements of particles and fields near Ganymede (e.g. signatures of reconnection), or  
530 observations of the incoming Jovian magnetospheric plasma via energetic neutral atoms (ENAs)  
531 imaging, to simultaneous multi-wavelengths remote sensing observations of its auroral footprint on  
532 Jupiter. Such observations will be instrumental to discriminate the many processes involved in the  
533 electrodynamic interaction and solve the questions listed here above.

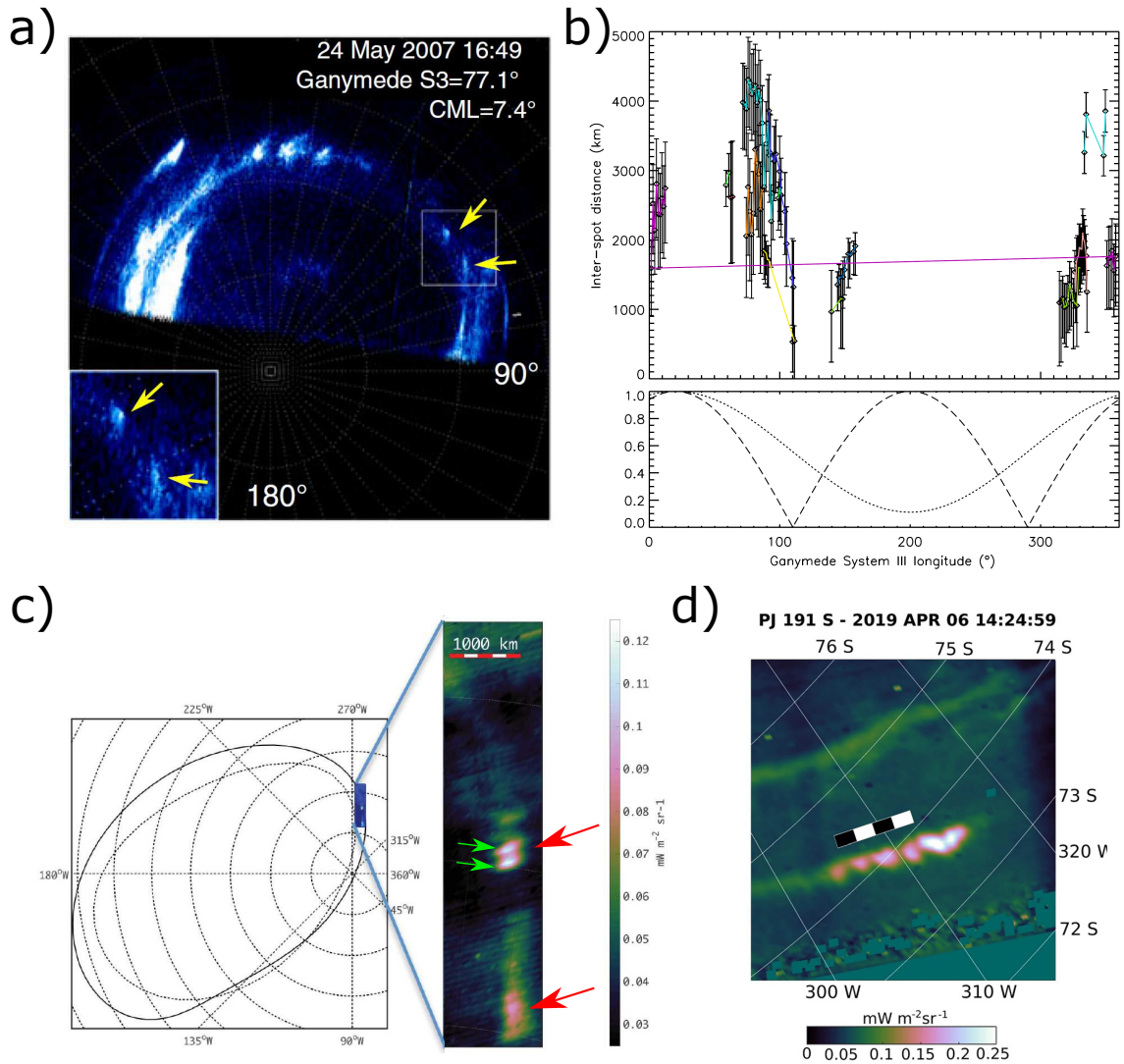


Figure 3.4: (a) Polar projections of an HST UV image acquired on 24 May 2007 at 16:40 UT. Two Ganymede footprint spots can be identified, as highlighted by the arrows. (b) Inter-spot distance between the two spots of the Ganymede footprint. (top) The colored lines connect points from the same HST orbit. The error bars assume a selection uncertainty of 1 pixel for the first spot and 2 pixels for the second one. (bottom) The long-dashed lines show the expected dependence of the distance for a trans-hemispheric electron beam spot (arbitrary units). In this case, the two spots merged as Ganymede crossed the centrifugal equator. The short-dashed line shows the expected behavior of the distance for a reflected Alfvén wing (RAW) spot. In this case, the minimum distance is expected when Ganymede is at its northernmost centrifugal latitude ( $\sim 200^\circ$  System III longitude). (from Bonfond et al. [2013]) c) Infrared image of the Ganymede footprint spots from the JIRAM instrument on board Juno. We can see each spot (red arrows) is actually formed of at least two sub-structures (green arrows). (from Mura et al. [2018]) d) Infrared images of the Ganymede footprint tail. The tail is also made of a string of sub-spots. (from Moirano et al. [2021])

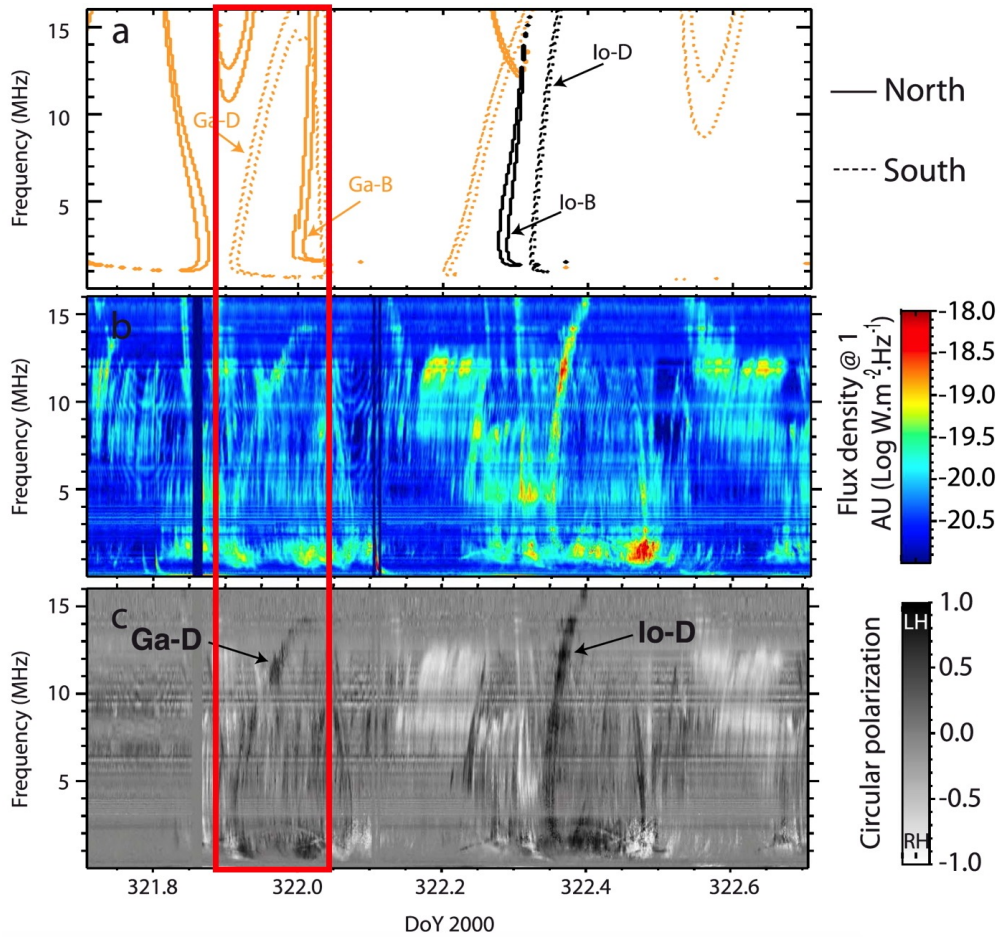


Figure 3.5: (a) ExPRES simulations of Io-induced (in black) and Ganymede-induced (in orange) radio arcs (solid line: northern emissions; dotted line, southern emissions) that should be detected by Cassini during its distant Jupiter flyby of 2000. (b) Dynamic spectrum of flux densities and (c) circular polarization measured by Cassini (LH = left-handed emission from the southern hemisphere; RH = right handed from the northern one). A southern Ganymede D arc is clearly recognized. The background of nested smaller arcs is of auroral origin. From Louis, Lamy, Zarka, Cecconi and Hess [2017].

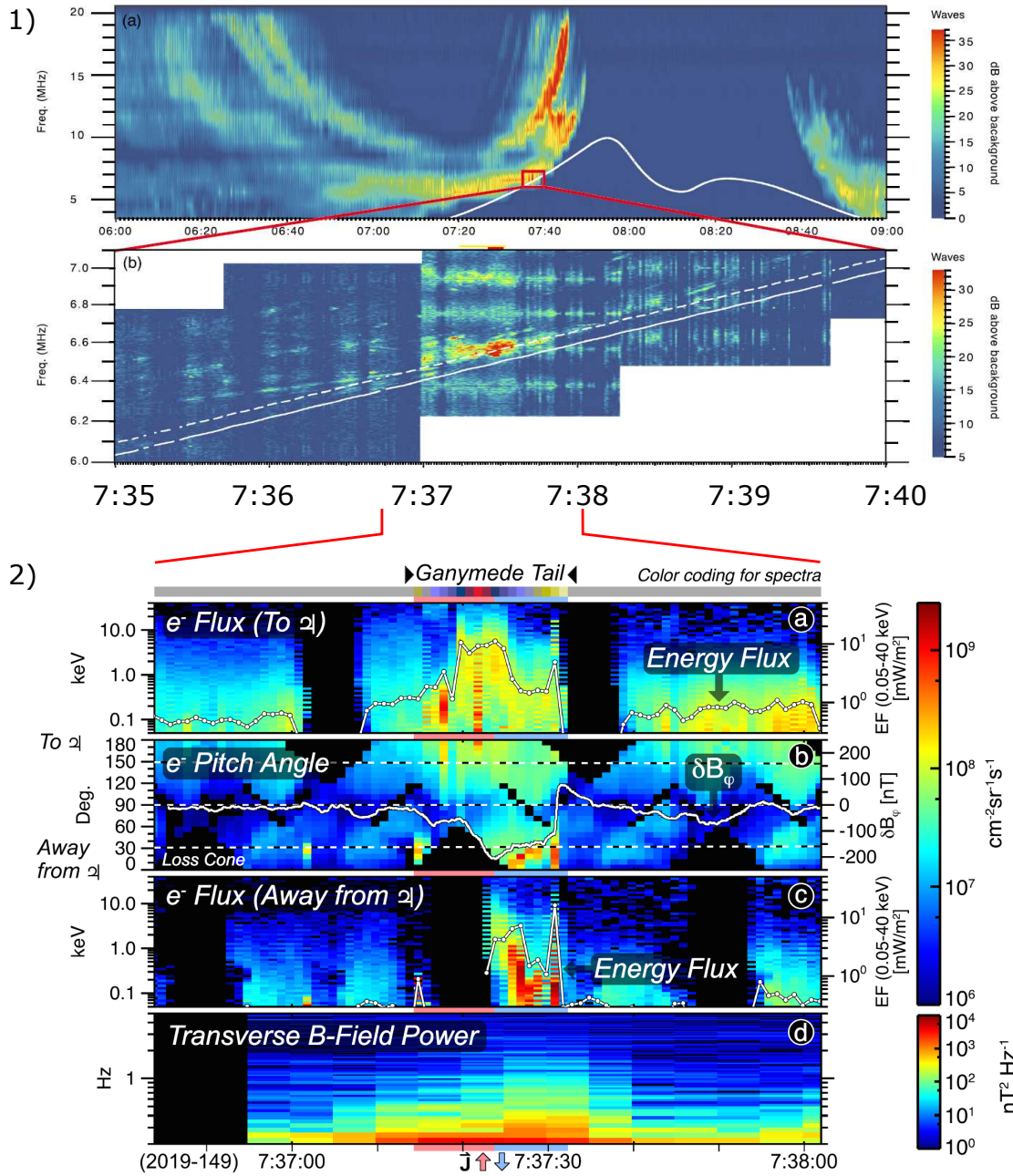


Figure 3.6: JADE, MAG and WAVES data during the Ganymede footprint tail flux tube encounter of 2019. (1a) Low resolution Juno/Waves data and (1b) zoom at high-resolution. The solid-white lines is the electron cyclotron frequency  $f_{ce}$  measured by Juno’s magnetometer, and the dashed white line is  $1.01 \times f_{ce}$  (adapted from Louis et al. [2020]). Panels (2a) and (2c) show the downward and upward electron differential energy flux (DEF) within the loss cone, respectively. Precipitating energy flux is overlaid on these panels with its separate axes on the right of the spectrograms. Panel (2b) shows electron pitch angles with  $\delta B_\phi$  overlaid. Panel (2d) shows the transverse B field power spectral densities. Red/blue bars indicate approximate upward/downward current regions inferred from MAG data. (from Szalay, Allegrini, Bagenal, Bolton, Bonfond, Clark, Connerney, Ebert, Gershman, Giles, Gladstone, Greathouse, Hospodarsky, Imai, Kurth, Kotsiaros, Louarn, McComas, Saur, Sulaiman and Wilson [2020])



## 534 Bibliography

- 535 Allegrini, F., Gladstone, G. R., Hue, V., Clark, G., Szalay, J. R., Kurth, W. S., Bagenal, F.,  
536 Bolton, S., Connerney, J. E. P., Ebert, R. W., Greathouse, T. K., Hospodarsky, G. B., Imai,  
537 M., Louarn, P., Mauk, B. H., McComas, D. J., Saur, J., Sulaiman, A. H., Valek, P. W.  
538 and Wilson, R. J. [2020], ‘First Report of Electron Measurements During a Europa Foot-  
539 print Tail Crossing by Juno’, *Geophysical Research Letters* **47**(18), e2020GL089732. \_eprint:  
540 <https://agupubs.onlinelibrary.wiley.com/doi/pdf/10.1029/2020GL089732>.  
541 **URL:** <https://agupubs.onlinelibrary.wiley.com/doi/abs/10.1029/2020GL089732>
- 542 Badman, S. V., Branduardi-Raymont, G., Galand, M., Hess, S. L. G., Krupp, N., Lamy, L., Melin,  
543 H. and Tao, C. [2015], ‘Auroral Processes at the Giant Planets: Energy Deposition, Emission  
544 Mechanisms, Morphology and Spectra’, *Space Science Reviews* **187**(1), 99–179.  
545 **URL:** <https://doi.org/10.1007/s11214-014-0042-x>
- 546 Bhattacharyya, D., Clarke, J. T., Montgomery, J., Bonfond, B., Gérard, J.-C. and Grodent, D.  
547 [2018], ‘Evidence for Auroral Emissions From Callisto’s Footprint in HST UV Images’, *Journal*  
548 *of Geophysical Research: Space Physics* **123**(1), 364–373.  
549 **URL:** <https://agupubs.onlinelibrary.wiley.com/doi/abs/10.1002/2017JA024791>
- 550 Bigg, E. K. [1964], ‘Influence of the Satellite Io on Jupiter’s Decametric Emission’, *Nature*  
551 **203**(4949), 1008–1010.  
552 **URL:** <https://www.nature.com/articles/2031008a0>
- 553 Bigg, E. K. [1966], ‘Periodicities in Jupiter’s decametric radiation’, *Planet. Space Sci.* **14**(8), 741–  
554 758.
- 555 Bonfond, B., Gérard, J.-C., Grodent, D. and Saur, J. [2007], ‘Ultraviolet Io footprint short timescale  
556 dynamics’, *Geophysical Research Letters* **34**(6).  
557 **URL:** <https://agupubs.onlinelibrary.wiley.com/doi/abs/10.1029/2006GL028765>

- 558 Bonfond, B., Grodent, D., Badman, S. V., Saur, J., Gérard, J. C. and Radioti, A. [2017], ‘Similarity  
559 of the Jovian satellite footprints: Spots multiplicity and dynamics’, *Icarus* **292**, 208–217.  
560 **URL:** <https://www.sciencedirect.com/science/article/pii/S0019103516304547>
- 561 Bonfond, B., Grodent, D., Gérard, J.-C., Radioti, A., Dols, V., Delamere, P. A. and Clarke, J. T.  
562 [2009], ‘The Io UV footprint: Location, inter-spot distances and tail vertical extent’, *Journal of*  
563 *Geophysical Research: Space Physics* **114**(A7).  
564 **URL:** <https://agupubs.onlinelibrary.wiley.com/doi/abs/10.1029/2009JA014312>
- 565 Bonfond, B., Grodent, D., Gérard, J.-C., Stallard, T., Clarke, J. T., Yoneda, M., Radioti, A. and  
566 Gustin, J. [2012], ‘Auroral evidence of Io’s control over the magnetosphere of Jupiter’, *Geophysical*  
567 *Research Letters* **39**(1).  
568 **URL:** <https://agupubs.onlinelibrary.wiley.com/doi/abs/10.1029/2011GL050253>
- 569 Bonfond, B., Hess, S., Bagenal, F., Gérard, J.-C., Grodent, D., Radioti, A., Gustin, J. and Clarke,  
570 J. T. [2013], ‘The multiple spots of the Ganymede auroral footprint’, *Geophysical Research Letters*  
571 **40**(19), 4977–4981.  
572 **URL:** <https://agupubs.onlinelibrary.wiley.com/doi/abs/10.1002/grl.50989>
- 573 Bonfond, B., Saur, J., Grodent, D., Badman, S. V., Bisikalo, D., Shematovich, V., Gérard, J.-C. and  
574 Radioti, A. [2017], ‘The tails of the satellite auroral footprints at Jupiter’, *Journal of Geophysical*  
575 *Research: Space Physics* **122**(8), 7985–7996.  
576 **URL:** <https://agupubs.onlinelibrary.wiley.com/doi/abs/10.1002/2017JA024370>
- 577 Chust, T., Roux, A., Kurth, W. S., Gurnett, D. A., Kivelson, M. G. and Khurana, K. K. [2005], ‘Are  
578 Io’s Alfvén wings filamented? Galileo observations’, *Planetary and Space Science* **53**(4), 395–412.  
579 **URL:** <http://www.sciencedirect.com/science/article/pii/S003206330400159X>
- 580 Clark, G., Mauk, B. H., Kollmann, P., Szalay, J. R., Sulaiman, A. H., Gershman, D. J., Saur, J.,  
581 Janser, S., Garcia-Sage, K., Greathouse, T., Paranicas, C., Allegrini, F., Bagenal, F., Bolton,  
582 S. J., Connerney, J. E. P., Ebert, R. W., Hospodarsky, G., Haggerty, D., Hue, V., Imai, M.,  
583 Kotsiaros, S., McComas, D. J., Rymer, A. and Westlake, J. [2020], ‘Energetic Proton Acceleration  
584 Associated With Io’s Footprint Tail’, *Geophysical Research Letters* **47**(24), e2020GL090839.  
585 **\_\_eprint:** <https://agupubs.onlinelibrary.wiley.com/doi/pdf/10.1029/2020GL090839>.  
586 **URL:** <https://onlinelibrary.wiley.com/doi/abs/10.1029/2020GL090839>

- 587 Clarke, J. T., Ajello, J., Ballester, G., Jaffel, L. B., Connerney, J., Gérard, J.-C., Gladstone, G. R.,  
588 Grodent, D., Pryor, W., Trauger, J. and Jr, J. H. W. [2002], ‘Ultraviolet emissions from the  
589 magnetic footprints of Io, Ganymede and Europa on Jupiter’, *Nature* **415**(6875), 997–1000.  
590 **URL:** <https://www.nature.com/articles/415997a>
- 591 Collinson, G., Paterson, W. R., Bard, C., Dorelli, J., Gloer, A., Sarantos, M. and Wil-  
592 son, R. [2018], ‘New Results From Galileo’s First Flyby of Ganymede: Reconnection-  
593 Driven Flows at the Low-Latitude Magnetopause Boundary, Crossing the Cusp, and  
594 Icy Ionospheric Escape’, *Geophysical Research Letters* **45**(8), 3382–3392. [\\_eprint:](#)  
595 <https://agupubs.onlinelibrary.wiley.com/doi/pdf/10.1002/2017GL075487>.  
596 **URL:** <https://agupubs.onlinelibrary.wiley.com/doi/abs/10.1002/2017GL075487>
- 597 Connerney, J. E. P. [1981], ‘The magnetic field of Jupiter: A generalized inverse approach’, *Journal*  
598 *of Geophysical Research: Space Physics* **86**(A9), 7679–7693.  
599 **URL:** <https://agupubs.onlinelibrary.wiley.com/doi/abs/10.1029/JA086iA09p07679>
- 600 Connerney, J. E. P., Acuña, M. H., Ness, N. F. and Satoh, T. [1998], ‘New models of Jupiter’s  
601 magnetic field constrained by the Io flux tube footprint’, *Journal of Geophysical Research: Space*  
602 *Physics* **103**(A6), 11929–11939.  
603 **URL:** <https://agupubs.onlinelibrary.wiley.com/doi/abs/10.1029/97JA03726>
- 604 Connerney, J. E. P., Baron, R., Satoh, T. and Owen, T. [1993], ‘Images of Excited  $H_{\alpha}$  at the  
605 Foot of the Io Flux Tube in Jupiter’s Atmosphere’, *Science* **262**(5136), 1035–1038.  
606 **URL:** <https://science.sciencemag.org/content/262/5136/1035>
- 607 Connerney, J. E. P., Kotsiaros, S., Oliverson, R. J., Espley, J. R., Joergensen, J. L., Joergensen,  
608 P. S., Merayo, J. M. G., Herceg, M., Bloxham, J., Moore, K. M., Bolton, S. J. and Levin, S. M.  
609 [2018], ‘A New Model of Jupiter’s Magnetic Field From Juno’s First Nine Orbits’, *Geophysical*  
610 *Research Letters* **45**(6), 2590–2596.  
611 **URL:** <https://agupubs.onlinelibrary.wiley.com/doi/abs/10.1002/2018GL077312>
- 612 Damiano, P. A., Delamere, P. A., Stauffer, B., Ng, C.-S. and Johnson, J. R.  
613 [2019], ‘Kinetic Simulations of Electron Acceleration by Dispersive Scale Alfvén Waves  
614 in Jupiter’s Magnetosphere’, *Geophysical Research Letters* **46**(6), 3043–3051. [\\_eprint:](#)  
615 <https://agupubs.onlinelibrary.wiley.com/doi/pdf/10.1029/2018GL081219>.  
616 **URL:** <https://agupubs.onlinelibrary.wiley.com/doi/abs/10.1029/2018GL081219>

- 617 Delamere, P. A., Bagenal, F., Ergun, R. and Su, Y.-J. [2003], ‘Momentum transfer between the Io  
618 plasma wake and Jupiter’s ionosphere’, *Journal of Geophysical Research: Space Physics* **108**(A6).  
619 **URL:** <https://agupubs.onlinelibrary.wiley.com/doi/abs/10.1029/2002JA009530>
- 620 Dulk, G. A. [1967], ‘Lack of Effects of Satellites Europa, Ganymede, Callisto, and Amalthea on the  
621 Decametric Radio Emission of Jupiter’, *Astrophys. J.* **148**, 239.
- 622 Ergun, R. E., Su, Y.-J., Andersson, L., Bagenal, F., Delemere, P. A., Lysak, R. L. and Strangeway,  
623 R. J. [2006], ‘S bursts and the Jupiter ionospheric Alfvén resonator’, *Journal of Geophysical  
624 Research: Space Physics* **111**(A6).  
625 **URL:** <https://agupubs.onlinelibrary.wiley.com/doi/abs/10.1029/2005JA011253>
- 626 Goldreich, P. and Lynden-Bell, D. [1969], ‘Io, a jovian unipolar inductor’, *Astrophys. Journal*  
627 **156**, 59–78.
- 628 Grasset, O., Dougherty, M. K., Coustenis, A., Bunce, E. J., Erd, C., Titov, D., Blanc, M., Coates,  
629 A., Drossart, P., Fletcher, L. N., Hussmann, H., Jaumann, R., Krupp, N., Lebreton, J. P., Prieto-  
630 Ballesteros, O., Tortora, P., Tosi, F. and Van Hoolst, T. [2013], ‘JUperiter ICy moons Explorer  
631 (JUICE): An ESA mission to orbit Ganymede and to characterise the Jupiter system’, *Planetary  
632 and Space Science* **78**, 1–21.  
633 **URL:** <https://www.sciencedirect.com/science/article/pii/S0032063312003777>
- 634 Grodent, D., Bonfond, B., Gérard, J.-C., Radioti, A., Gustin, J., Clarke, J. T., Nichols, J. and  
635 Connerney, J. E. P. [2008], ‘Auroral evidence of a localized magnetic anomaly in Jupiter’s northern  
636 hemisphere’, *Journal of Geophysical Research: Space Physics* **113**(A9).  
637 **URL:** <https://agupubs.onlinelibrary.wiley.com/doi/abs/10.1029/2008JA013185>
- 638 Grodent, D., Bonfond, B., Radioti, A., Gérard, J.-C., Jia, X., Nichols, J. D. and Clarke, J. T. [2009],  
639 ‘Auroral footprint of Ganymede’, *Journal of Geophysical Research: Space Physics* **114**(A7).  
640 **URL:** <https://agupubs.onlinelibrary.wiley.com/doi/abs/10.1029/2009JA014289>
- 641 Grodent, D., Gérard, J.-C., Radioti, A., Bonfond, B. and Saglam, A. [2008], ‘Jupiter’s chang-  
642 ing auroral location’, *Journal of Geophysical Research: Space Physics* **113**(A1). [\\_eprint:  
643 https://agupubs.onlinelibrary.wiley.com/doi/pdf/10.1029/2007JA012601](https://agupubs.onlinelibrary.wiley.com/doi/pdf/10.1029/2007JA012601).  
644 **URL:** <https://agupubs.onlinelibrary.wiley.com/doi/abs/10.1029/2007JA012601>

- 645 Gurnett, D. A. and Goertz, C. K. [1981], ‘Multiple Alfvén wave reflections excited by Io Origin of  
646 the Jovian decametric arcs’, *J. Geophys. Res.* **86**, 717–722.
- 647 Gurnett, D. A., Kurth, W. S., Roux, A., Bolton, S. J. and Kennel, C. F. [1996], ‘Evidence for a  
648 magnetosphere at Ganymede from plasma-wave observations by the Galileo spacecraft’, *Nature*  
649 **384**(6609), 535–537. Number: 6609 Publisher: Nature Publishing Group.  
650 **URL:** <https://www.nature.com/articles/384535a0>
- 651 Gustin, J., Bonfond, B., Grodent, D. and Gérard, J.-C. [2012], ‘Conversion from HST ACS and  
652 STIS auroral counts into brightness, precipitated power, and radiated power for H<sub>2</sub> giant planets’,  
653 *Journal of Geophysical Research: Space Physics* **117**(A7).  
654 **URL:** <https://agupubs.onlinelibrary.wiley.com/doi/abs/10.1029/2012JA017607>
- 655 Hess, S., Bonfond, B., Bagenal, F. and Lamy, L. [2017], ‘A model of the Jovian internal field derived  
656 from in-situ and auroral constraints’. Publisher: Austrian Academy of Sciences Press.  
657 **URL:** <https://orbi.uliege.be/handle/2268/221222>
- 658 Hess, S. and Delamere, P. [2012], Satellite-Induced Electron Acceleration and Related Auroras, *in*  
659 A. Keiling, E. Donovan, F. Bagenal and T. Karlsson, eds, ‘Auroral Phenomenology and Magne-  
660 topheric Processes: Earth And Other Planets’, American Geophysical Union.  
661 **URL:** <http://onlinelibrary.wiley.com/doi/10.1029/2011GM001175/summary>
- 662 Hess, S. L. G., Bonfond, B., Chantry, V., Gérard, J. C., Grodent, D., Jacobsen, S. and Radioti,  
663 A. [2013], ‘Evolution of the Io footprint brightness II: Modeling’, *Planetary and Space Science*  
664 **88**, 76–85.  
665 **URL:** <http://www.sciencedirect.com/science/article/pii/S0032063313002109>
- 666 Hess, S. L. G., Bonfond, B. and Delamere, P. A. [2013], ‘How could the Io footprint disappear?’,  
667 *Planetary and Space Science* **89**, 102–110.  
668 **URL:** <http://www.sciencedirect.com/science/article/pii/S0032063313002195>
- 669 Hess, S. L. G., Delamere, P., Dols, V., Bonfond, B. and Swift, D. [2010], ‘Power transmission and  
670 particle acceleration along the Io flux tube’, *Journal of Geophysical Research: Space Physics*  
671 **115**(A6).  
672 **URL:** <https://agupubs.onlinelibrary.wiley.com/doi/abs/10.1029/2009JA014928>

- 673 Hess, S., Mottez, F. and Zarka, P. [2007], ‘Jovian S burst generation by Alfvén waves’, *Journal of*  
674 *Geophysical Research (Space Physics)* **112**(A11), A11212.
- 675 Hess, S., Mottez, F., Zarka, P. and Chust, T. [2008], ‘Generation of the jovian radio decametric arcs  
676 from the Io Flux Tube’, *Journal of Geophysical Research (Space Physics)* **113**(A3), A03209.
- 677 Hess, S., Zarka, P. and Mottez, F. [2007], ‘Io Jupiter interaction, millisecond bursts and field-aligned  
678 potentials’, *Planet. Space Sci.* **55**, 89–99.
- 679 Hess, S., Zarka, P., Mottez, F. and Ryabov, V. B. [2009], ‘Electric potential jumps in the Io-Jupiter  
680 flux tube’, *Planetary and Space Science* **57**(1), 23–33.  
681 **URL:** <http://www.sciencedirect.com/science/article/pii/S0032063308003358>
- 682 Higgins, C. A. [2007], ‘Satellite control of Jovian 2–6 MHz radio emission using Voy-  
683 ager data’, *Journal of Geophysical Research: Space Physics* **112**(A5). [\\_eprint:](#)  
684 <https://agupubs.onlinelibrary.wiley.com/doi/pdf/10.1029/2006JA012100>.  
685 **URL:** <https://agupubs.onlinelibrary.wiley.com/doi/abs/10.1029/2006JA012100>
- 686 Hill, T. W. and Vasyliunas, V. M. [2002], ‘Jovian auroral signature of Io’s corotational wake’, *J.*  
687 *Geophys. Res.* **107**(A12), 27–1.
- 688 Hinson, D. P., Kliore, A. J., Flasar, F. M., Twicken, J. D., Schinder, P. J. and Herrera, R. G. [1998],  
689 ‘Galileo radio occultation measurements of Io’s ionosphere and plasma wake’, *J. Geophys. Res.*  
690 **103**, 29343–29358.
- 691 Hinton, P. C., Bagenal, F. and Bonfond, B. [2019], ‘Alfvén Wave Propagation in  
692 the Io Plasma Torus’, *Geophysical Research Letters* **46**(3), 1242–1249. [\\_eprint:](#)  
693 <https://agupubs.onlinelibrary.wiley.com/doi/pdf/10.1029/2018GL081472>.  
694 **URL:** <https://agupubs.onlinelibrary.wiley.com/doi/abs/10.1029/2018GL081472>
- 695 Hospodarsky, G. B., Christopher, I. W., Menietti, J. D., Kurth, W. S., Gurnett, D. A., Averkamp,  
696 T. F., Groene, J. B. and Zarka, P. [2001], Control of Jovian Radio Emissions by the Galilean  
697 Moons as Observed by Cassini and Galileo, *in* ‘Planetary Radio Emissions V’, pp. 155–164.
- 698 Jacobsen, S., Neubauer, F. M., Saur, J. and Schilling, N. [2007], ‘Io’s nonlinear MHD-wave field in  
699 the heterogeneous Jovian magnetosphere’, *Geophys. Res. Lett.* **34**, 10202–+.

- 700 Jacobsen, S., Saur, J., Neubauer, F. M., Bonfond, B., Gérard, J.-C. and Grodent, D. [2010], ‘Loca-  
701 tion and spatial shape of electron beams in Io’s wake’, *J. Geophys. Res.* **115**(A14), A04205.
- 702 Jia, X., Walker, R. J., G, K. M., Khurana, K. K. and Linker, J. A. [2009], ‘Properties of Ganymede’s  
703 magnetosphere inferred from improved three-dimensional MHD simulations’, *J. Geophys. Res.*  
704 **114**, A09209.
- 705 Jia, X., Walker, R. J., Kivelson, M. G., Khurana, K. K. and Linker, J. A. [2008], ‘Three-dimensional  
706 MHD simulations of Ganymede’s magnetosphere’, *J. Geophys. Res.* **113**(A12), 6212–+.
- 707 Jia, X., Walker, R. J., Kivelson, M. G., Khurana, K. K. and Linker, J. A. [2010], ‘Dynamics of  
708 Ganymede’s magnetopause: Intermittent reconnection under steady external conditions’, *Journal*  
709 *of Geophysical Research (Space Physics)* **115**(A14), A12202.
- 710 Jones, S. T. and Su, Y.-J. [2008], ‘Role of dispersive Alfvén waves in generating parallel electric  
711 fields along the Io-Jupiter fluxtube’, *J. Geophys. Res.* **113**(A12), 12205–+.
- 712 Kaiser, M. L. and Alexander, J. K. [1973], ‘Periodicities in the Jovian Decametric Emission’, *As-  
713 trophys. Lett.* **14**, 55.
- 714 Kaiser, M. L. and MacDowall, R. J. [1998], ‘Jovian radio “bullseyes” observed by Ulysses’, *Geophys.  
715 Res. Lett.* **25**(16), 3113–3116.
- 716 Kaweeyanun, N., Masters, A. and Jia, X. [2020], ‘Favorable Conditions for Magnetic Reconnection  
717 at Ganymede’s Upstream Magnetopause’, *Geophysical Research Letters* **47**(6), e2019GL086228.  
718 \_eprint: <https://agupubs.onlinelibrary.wiley.com/doi/pdf/10.1029/2019GL086228>.  
719 **URL:** <https://agupubs.onlinelibrary.wiley.com/doi/abs/10.1029/2019GL086228>
- 720 Khurana, K. K. [1997], ‘Euler potential models of Jupiter’s magnetospheric field’, *Journal of Geo-  
721 physical Research: Space Physics* **102**(A6), 11295–11306.  
722 **URL:** <https://agupubs.onlinelibrary.wiley.com/doi/abs/10.1029/97JA00563>
- 723 Kivelson, M. G. and Bagenal, F. [2014], Chapter 7 - Planetary Magnetospheres, *in* T. Spohn,  
724 D. Breuer and T. V. Johnson, eds, ‘Encyclopedia of the Solar System (Third Edition)’, Elsevier,  
725 Boston, pp. 137–157.  
726 **URL:** <http://www.sciencedirect.com/science/article/pii/B9780124158450000074>

- 727 Kivelson, M. G., Bagenal, F., Kurth, W. S., Neubauer, F. M., Paranicas, C. and Saur, J. [2004],  
728 Magnetospheric interactions with satellites, *in* ‘Jupiter. The Planet, Satellites and Magneto-  
729 sphere’, Jupiter. The Planet, Satellites and Magnetosphere, pp. 513–536. Citation Key Alias:  
730 kivelsonMagnetosphericInteractionsSatellites.
- 731 Kivelson, M. G., Warnecke, J., Bennett, L., Joy, S., Khurana, K. K., Linker, J. A., Rus-  
732 sell, C. T., Walker, R. J. and Polanskey, C. [1998], ‘Ganymede’s magnetosphere: Magne-  
733 tometer overview’, *Journal of Geophysical Research: Planets* **103**(E9), 19963–19972. \_eprint:  
734 <https://agupubs.onlinelibrary.wiley.com/doi/pdf/10.1029/98JE00227>.  
735 **URL:** <https://agupubs.onlinelibrary.wiley.com/doi/abs/10.1029/98JE00227>
- 736 Kurth, W. S., Bolton, S. J., Gurnett, D. A. and Levin, S. [1997], ‘A determination of the source of  
737 Jovian hectometric radiation via occultation by Ganymede’, *Geophys. Res. Lett.* **24**(10), 1171–  
738 1174.
- 739 Kurth, W. S., Gurnett, D. A. and Menietti, J. D. [2000], ‘The Influence of the Galilean Satel-  
740 lites on Radio Emissions from the Jovian System’, *Washington DC American Geophysical Union*  
741 *Geophysical Monograph Series* **119**, 213.
- 742 Kurth, W. S., Gurnett, D. A., Roux, A. and Bolton, S. J. [1997], ‘Ganymede:  
743 A new radio source’, *Geophysical Research Letters* **24**(17), 2167–2170. \_eprint:  
744 <https://agupubs.onlinelibrary.wiley.com/doi/pdf/10.1029/97GL02249>.  
745 **URL:** <https://agupubs.onlinelibrary.wiley.com/doi/abs/10.1029/97GL02249>
- 746 Lamy, L., Zarka, P., Cecconi, B., Klein, L., Masson, S., Denis, L., Coffre, A. and Viou, C. [2017],  
747 1977-2017: 40 years of decametric observations of Jupiter and the Sun with the Nancay Decameter  
748 Array, *in* G. Fischer, G. Mann, M. Panchenko and P. Zarka, eds, ‘Planetary Radio Emissions  
749 VIII’, pp. 455–466.
- 750 Lavrukhin, A. S. and Alexeev, I. I. [2015], ‘Aurora at high latitudes of Ganymede’, *Astronomy*  
751 *Letters* **41**(11), 687–692.  
752 **URL:** <https://doi.org/10.1134/S1063773715110043>
- 753 Le Quéau, D. [1988], Planetary radio emissions from high magnetic latitudes: The “Cyclotron-  
754 Maser” theory, *in* ‘Planetary Radio Emissions II’, Austrian Acad. Sci. Press, Graz, Austria,



- 755 pp. pp. 381–398.  
756 **URL:** <http://www.austriaca.at:8080/1523-6inhalt?frames=yes>
- 757 Lebo, G. R., Smith, A. G. and Carr, T. D. [1965], ‘Jupiter’s Decametric Emission Correlated with  
758 the Longitudes of the First Three Galilean Satellites’, *Science* **148**(3678), 1724–1725. Publisher:  
759 American Association for the Advancement of Science Section: Reports.  
760 **URL:** <https://science.sciencemag.org/content/148/3678/1724>
- 761 Louis, C. K., Hess, S. L. G., Cecconi, B., Zarka, P., Lamy, L., Aicardi, S. and Loh, A. [2019], ‘Ex-  
762 PRES: an Exoplanetary and Planetary Radio Emissions Simulator’, *Astron. Astrophys.* **627**, A30.
- 763 Louis, C. K., Lamy, L., Zarka, P., Cecconi, B. and Hess, S. L. G. [2017], ‘Detection of  
764 Jupiter decametric emissions controlled by Europa and Ganymede with Voyager/PRA and  
765 Cassini/RPWS’, *Journal of Geophysical Research: Space Physics* **122**(9), 9228–9247. \_eprint:  
766 <https://agupubs.onlinelibrary.wiley.com/doi/pdf/10.1002/2016JA023779>.  
767 **URL:** <https://agupubs.onlinelibrary.wiley.com/doi/abs/10.1002/2016JA023779>
- 768 Louis, C. K., Louarn, P., Allegrini, F., Kurth, W. S. and Szalay, J. R. [2020],  
769 ‘Ganymede-Induced Decametric Radio Emission: In Situ Observations and Measure-  
770 ments by Juno’, *Geophysical Research Letters* **47**(20), e2020GL090021. \_eprint:  
771 <https://agupubs.onlinelibrary.wiley.com/doi/pdf/10.1029/2020GL090021>.  
772 **URL:** <https://agupubs.onlinelibrary.wiley.com/doi/abs/10.1029/2020GL090021>
- 773 Louis, C., Lamy, L., Zarka, P., Cecconi, B., Hess, S. L. G. and Bonnin, X. [2017], Simulating  
774 Jupiter-satellite decametric emissions with ExPRES: A parametric study, in G. Fischer, G. Mann,  
775 M. Panchenko and P. Zarka, eds, ‘Planetary Radio Emissions VIII’, pp. 59–72.
- 776 Marques, M. S., Zarka, P., Echer, E., Ryabov, V. B., Alves, M. V., Denis, L. and Coffre, A. [2017],  
777 ‘Statistical analysis of 26 yr of observations of decametric radio emissions from Jupiter’, *Astron.*  
778 *Astrophys.* **604**, A17.
- 779 Matsuda, K., Terada, N., Katoh, Y. and Misawa, H. [2012], ‘A simulation study of the current-  
780 voltage relationship of the Io tail aurora’, *Journal of Geophysical Research (Space Physics)*  
781 **117**(A16), 10214.
- 782 Mauk, B. H., Williams, D. J. and McEntire, R. W. [1997], ‘Energy-time dis-  
783 persed charged particle signatures of dynamic injections in Jupiter’s inner

- 784 magnetosphere’, *Geophysical Research Letters* **24**(23), 2949–2952. [\\_eprint:](#)  
785 <https://agupubs.onlinelibrary.wiley.com/doi/pdf/10.1029/97GL03026>.  
786 **URL:** <https://agupubs.onlinelibrary.wiley.com/doi/abs/10.1029/97GL03026>
- 787 Menietti, J. D., Gurnett, D. A., Kurth, W. S. and Groene, J. B. [1998], ‘Control of Jo-  
788 vian radio emission by Ganymede’, *Geophysical Research Letters* **25**(23), 4281–4284. [\\_eprint:](#)  
789 <https://agupubs.onlinelibrary.wiley.com/doi/pdf/10.1029/1998GL900112>.  
790 **URL:** <https://agupubs.onlinelibrary.wiley.com/doi/abs/10.1029/1998GL900112>
- 791 Menietti, J. D., Gurnett, D. A., Kurth, W. S., Groene, J. B. and Granroth, L. J. [1998], ‘Galileo  
792 direction finding of Jovian radio emissions’, *J. Geophys. Res.* **103**(E9), 20001–20010.
- 793 Moirano, A., Mura, A., Adriani, A., Dols, V., Bonfond, B., Waite, J. H., Hue, V., Szalay,  
794 J. R., Sulaiman, A. H., Dinelli, B. M., Tosi, F., Altieri, F., Cicchetti, A., Filacchione, G.,  
795 Grassi, D., Migliorini, A., Moriconi, M. L., Noschese, R., Piccioni, G., Sordini, R., Tur-  
796 rini, D., Plainaki, C., Sindoni, G., Massetti, S., Lysak, R. L., Ivanovski, S. L. and Bolton,  
797 S. J. [2021], ‘Morphology of the Auroral Tail of Io, Europa, and Ganymede From JIRAM  
798 L-Band Imager’, *Journal of Geophysical Research: Space Physics* **126**(9), e2021JA029450.  
799 [\\_eprint:](#) <https://onlinelibrary.wiley.com/doi/pdf/10.1029/2021JA029450> tex.ids= moiranoMor-  
800 phologyAuroralTail.  
801 **URL:** <https://onlinelibrary.wiley.com/doi/abs/10.1029/2021JA029450>
- 802 Moore, K. M., Bloxham, J., Connerney, J. E. P., Jørgensen, J. L. and Merayo, J. M. G. [2017],  
803 ‘The analysis of initial Juno magnetometer data using a sparse magnetic field representation’,  
804 *Geophysical Research Letters* **44**, 4687–4693.
- 805 Mura, A., Adriani, A., Altieri, F., Connerney, J. E. P., Bolton, S. J., Moriconi, M. L., Gérard, J.-C.,  
806 Kurth, W. S., Dinelli, B. M., Fabiano, F., Tosi, F., Atreya, S. K., Bagenal, F., Gladstone, G. R.,  
807 Hansen, C., Levin, S. M., Mauk, B. H., McComas, D. J., Sindoni, G., Filacchione, G., Migliorini,  
808 A., Grassi, D., Piccioni, G., Noschese, R., Cicchetti, A., Turrini, D., Stefani, S., Amoroso, M. and  
809 Olivieri, A. [2017], ‘Infrared observations of Jovian aurora from Juno’s first orbits: Main oval and  
810 satellite footprints’, *Geophysical Research Letters* **44**, 5308–5316.
- 811 Mura, A., Adriani, A., Connerney, J. E. P., Bolton, S., Altieri, F., Bagenal, F., Bonfond, B., Dinelli,  
812 B. M., Gérard, J.-C., Greathouse, T., Grodent, D., Levin, S., Mauk, B., Moriconi, M. L., Saur,  
813 J., Waite, J. H., Amoroso, M., Cicchetti, A., Fabiano, F., Filacchione, G., Grassi, D., Migliorini,

- 814 A., Noschese, R., Olivieri, A., Piccioni, G., Plainaki, C., Sindoni, G., Sordini, R., Tosi, F. and  
815 Turrini, D. [2018], ‘Juno observations of spot structures and a split tail in Io-induced aurorae on  
816 Jupiter’, *Science* **361**(6404), 774–777.  
817 **URL:** <http://science.sciencemag.org/content/361/6404/774>
- 818 Neubauer, F. M. [1980], ‘Nonlinear standing Alfvén wave current system at Io - Theory’, *J. Geophys.*  
819 *Res.* **85**, 1171–1178.
- 820 Neubauer, F. M. [1998], ‘The sub-Alfvénic interaction of the Galilean satellites with the Jovian  
821 magnetosphere’, *Journal of Geophysical Research: Planets* **103**(E9), 19843–19866. `_eprint:`  
822 <https://agupubs.onlinelibrary.wiley.com/doi/pdf/10.1029/97JE03370>.  
823 **URL:** <https://agupubs.onlinelibrary.wiley.com/doi/abs/10.1029/97JE03370>
- 824 Paranicas, C., Mauk, B. H., Haggerty, D. K., Clark, G., Kollmann, P., Rymer, A. M., West-  
825 lake, J., Allen, R. C., Szalay, J., Ebert, R. W., Sulaiman, A. H., Imai, M., Roussos, E.,  
826 Krupp, N., Nénon, Q., Bagenal, F. and Bolton, S. J. [2019], ‘Io’s Effect on Energetic Charged  
827 Particles as Seen in Juno Data’, *Geophysical Research Letters* **46**(23), 13615–13620. `_eprint:`  
828 <https://agupubs.onlinelibrary.wiley.com/doi/pdf/10.1029/2019GL085393>.  
829 **URL:** <https://agupubs.onlinelibrary.wiley.com/doi/abs/10.1029/2019GL085393>
- 830 Pryor, W. R., Rymer, A. M., Mitchell, D. G., Hill, T. W., Young, D. T., Saur, J., Jones, G. H.,  
831 Jacobsen, S., Cowley, S. W. H., Mauk, B. H., Coates, A. J., Gustin, J., Grodent, D., Gérard, J.-  
832 C., Lamy, L., Nichols, J. D., Krimigis, S. M., Esposito, L. W., Dougherty, M. K., Jouchoux, A. J.,  
833 Stewart, A. I. F., McClintock, W. E., Holsclaw, G. M., Ajello, J. M., Colwell, J. E., Hendrix,  
834 A. R., Crary, F. J., Clarke, J. T. and Zhou, X. [2011], ‘The auroral footprint of Enceladus on  
835 Saturn’, *Nature* **472**(7343), 331–333.  
836 **URL:** <https://www.nature.com/articles/nature09928>
- 837 Saur, J., Grambusch, T., Duling, S., Neubauer, F. M. and Simon, S. [2013], ‘Magnetic energy fluxes  
838 in sub-Alfvénic planet star and moon planet interactions’, *Astronomy & Astrophysics* **552**, A119.  
839 **URL:** <https://www.aanda.org/articles/aa/abs/2013/04/aa18179-11/aa18179-11.html>
- 840 Saur, J., Neubauer, F. M., Connerney, J. E. P., Zarka, P. and Kivelson, M. G. [2004], Plasma  
841 interaction of io with its plasma torus, in ‘Jupiter. The Planet, Satellites and Magnetosphere’,  
842 Jupiter. The Planet, Satellites and Magnetosphere, pp. 537–560. Citation Key Alias: saurPlas-  
843 maInteractionsIo.

- 844 St. Cyr, O. C. [1985], Jupiter's Decameter and Kilometer Emissions: Satellite Effects and Long  
845 Term Periodicities, PhD thesis, Florida Univ., Gainesville.
- 846 Su, Y.-J., Ergun, R. E., Bagenal, F. and Delamere, P. A. [2003], 'Io-related Jovian auroral arcs:  
847 Modeling parallel electric fields', *Journal of Geophysical Research: Space Physics* **108**(A2).  
848 **URL:** <https://agupubs.onlinelibrary.wiley.com/doi/abs/10.1029/2002JA009247>
- 849 Sulaiman, A. H., Hospodarsky, G. B., Elliott, S. S., Kurth, W. S., Gurnett, D. A., Imai, M.,  
850 Allegrini, F., Bonfond, B., Clark, G., Connerney, J. E. P., Ebert, R. W., Gershman, D. J., Hue,  
851 V., Janser, S., Kotsiaros, S., Paranicas, C., Santolik, O., Saur, J., Szalay, J. R. and Bolton, S. J.  
852 [2020], 'Wave-particle interactions associated with Io's auroral footprint: Evidence of Alfvén, ion  
853 cyclotron, and whistler modes', *Geophysical Research Letters* **n/a**(n/a), e2020GL088432. \_eprint:  
854 <https://agupubs.onlinelibrary.wiley.com/doi/pdf/10.1029/2020GL088432>.  
855 **URL:** <https://agupubs.onlinelibrary.wiley.com/doi/abs/10.1029/2020GL088432>
- 856 Szalay, J. R., Allegrini, F., Bagenal, F., Bolton, S. J., Bonfond, B., Clark, G., Connerney,  
857 J. E. P., Ebert, R. W., Gershman, D. J., Giles, R. S., Gladstone, G. R., Greathouse,  
858 T., Hospodarsky, G. B., Imai, M., Kurth, W. S., Kotsiaros, S., Louarn, P., McComas,  
859 D. J., Saur, J., Sulaiman, A. H. and Wilson, R. J. [2020], 'Alfvénic Acceleration Sus-  
860 tains Ganymede's Footprint Tail Aurora', *Geophysical Research Letters* **47**(3), e2019GL086527.  
861 \_eprint: <https://agupubs.onlinelibrary.wiley.com/doi/pdf/10.1029/2019GL086527>.  
862 **URL:** <https://agupubs.onlinelibrary.wiley.com/doi/abs/10.1029/2019GL086527>
- 863 Szalay, J. R., Bagenal, F., Allegrini, F., Bonfond, B., Clark, G., Connerney, J. E. P., Crary,  
864 F., Ebert, R. W., Ergun, R. E., Gershman, D. J., Hinton, P. C., Imai, M., Janser,  
865 S., McComas, D. J., Paranicas, C., Saur, J., Sulaiman, A. H., Thomsen, M. F., Wil-  
866 son, R. J., Bolton, S. and Levin, S. M. [2020], 'Proton Acceleration by Io's Alfvénic Inter-  
867 action', *Journal of Geophysical Research: Space Physics* **125**(1), e2019JA027314. \_eprint:  
868 <https://agupubs.onlinelibrary.wiley.com/doi/pdf/10.1029/2019JA027314>.  
869 **URL:** <https://agupubs.onlinelibrary.wiley.com/doi/abs/10.1029/2019JA027314>
- 870 Szalay, J. R., Bonfond, B., Allegrini, F., Bagenal, F., Bolton, S., Clark, G., Connerney, J. E. P.,  
871 Ebert, R. W., Ergun, R. E., Gladstone, G. R., Grodent, D., Hospodarsky, G. B., Hue, V., Kurth,  
872 W. S., Kotsiaros, S., Levin, S. M., Louarn, P., Mauk, B., McComas, D. J., Saur, J., Valek,  
873 P. W. and Wilson, R. J. [2018], 'In Situ Observations Connected to the Io Footprint Tail Aurora',

- 874 *Journal of Geophysical Research: Planets* **123**(11), 3061–3077.  
875 **URL:** <https://agupubs.onlinelibrary.wiley.com/doi/abs/10.1029/2018JE005752>
- 876 Vogt, M. F., Bunce, E. J., Kivelson, M. G., Khurana, K. K., Walker, R. J., Radioti, A., Bonfond,  
877 B. and Grodent, D. [2015], ‘Magnetosphere-ionosphere mapping at Jupiter: Quantifying the  
878 effects of using different internal field models’, *Journal of Geophysical Research: Space Physics*  
879 **120**(4), 2584–2599.  
880 **URL:** <https://agupubs.onlinelibrary.wiley.com/doi/abs/10.1002/2014JA020729>
- 881 Vogt, M. F., Kivelson, M. G., Khurana, K. K., Walker, R. J., Bonfond, B., Grodent, D. and Radioti,  
882 A. [2011], ‘Improved mapping of Jupiter’s auroral features to magnetospheric sources’, *Journal*  
883 *of Geophysical Research: Space Physics* **116**(A3).  
884 **URL:** <https://agupubs.onlinelibrary.wiley.com/doi/full/10.1029/2010JA016148>
- 885 Wannawichian, S., Clarke, J. T. and Nichols, J. D. [2010], ‘Ten years of Hubble Space Telescope  
886 observations of the variation of the Jovian satellites’ auroral footprint brightness’, *Journal of*  
887 *Geophysical Research: Space Physics* **115**(A2).  
888 **URL:** <https://agupubs.onlinelibrary.wiley.com/doi/abs/10.1029/2009JA014456>
- 889 Williams, D. J. and Mauk, B. [1997], ‘Pitch angle diffusion at Jupiter’s moon Ganymede’, *J. Geo-*  
890 *phys. Res.* **102**(A11), 24283–24302.
- 891 Williams, D. J., Mauk, B. H., McEntire, R. W., Roelof, E. C., Armstrong, T. P., Wilken, B.,  
892 Roederer, J. G., Krimigis, S. M., Fritz, T. A., Lanzerotti, L. J. and Murphy, N. [1997], ‘Energetic  
893 particle signatures at Ganymede: Implications for Ganymede’s magnetic field’, *Geophys. Res.*  
894 *Lett.* **24**(17), 2163–2166.
- 895 Yoneda, M., Kagitani, M. and Okano, S. [2009], ‘Short-term variability of Jupiter’s extended sodium  
896 nebula’, *Icarus* **204**(2), 589–596.  
897 **URL:** <http://www.sciencedirect.com/science/article/pii/S0019103509003157>
- 898 Yoneda, M., Tsuchiya, F., Misawa, H., Bonfond, B., Tao, C., Kagitani, M. and Okano, S. [2013],  
899 ‘Io’s volcanism controls Jupiter’s radio emissions’, *Geophysical Research Letters* **40**(4), 671–675.  
900 **URL:** <https://agupubs.onlinelibrary.wiley.com/doi/abs/10.1002/grl.50095>
- 901 Zarka, P. [1998], ‘Auroral radio emissions at the outer planets: Observations and theories’, *Journal*

- 902 of *Geophysical Research: Planets* **103**(E9), 20159–20194.  
903 **URL:** <https://agupubs.onlinelibrary.wiley.com/doi/abs/10.1029/98JE01323>
- 904 Zarka, P. [2007], ‘Plasma interactions of exoplanets with their parent star and associated radio  
905 emissions’, *Planet. Space Sci.* **55**(5), 598–617.
- 906 Zarka, P. [2020], Star-Planet Interactions in the Radio Domain: Prospect for Their Detection, *in*  
907 H. J. Deeg and J. A. Belmonte, eds, ‘Handbook of Exoplanets’, Springer International Publishing,  
908 Cham, pp. 1–16.  
909 **URL:** [https://doi.org/10.1007/978-3-319-30648-3\\_22-2](https://doi.org/10.1007/978-3-319-30648-3_22-2)
- 910 Zarka, P., Marques, M. S., Louis, C., Ryabov, V. B., Lamy, L., Echer, E. and Cecconi, B. [2018],  
911 ‘Jupiter radio emission induced by Ganymede and consequences for the radio detection of exo-  
912 planets’, *Astronomy & Astrophysics* **618**, A84. tex.ids: zarkaJupiterRadioEmission2018 publisher:  
913 EDP Sciences.  
914 **URL:** <https://www.aanda.org/articles/aa/abs/2018/10/aa33586-18/aa33586-18.html>
- 915 Zarka, P., Treumann, R. A., Ryabov, B. P. and Ryabov, V. B. [2001], ‘Magnetically-Driven Plane-  
916 tary Radio Emissions and Application to Extrasolar Planets’, *Astrophys. Space Sci.* **277**, 293–300.
- 917 Zhou, H., Tóth, G., Jia, X. and Chen, Y. [2020], ‘Reconnection-Driven Dynamics at Ganymede’s  
918 Upstream Magnetosphere: 3-D Global Hall MHD and MHD-EPIC Simulations’, *Journal of Geo-  
919 physical Research (Space Physics)* **125**(8), e28162.
- 920 Zhou, H., Tóth, G., Jia, X., Chen, Y. and Markidis, S. [2019], ‘Embedded Kinetic Simulation  
921 of Ganymede’s Magnetosphere: Improvements and Inferences’, *Journal of Geophysical Research  
922 (Space Physics)* **124**(7), 5441–5460.